☙

Conceptual designs of two petawatt-class pulsed-power accelerators for high-energy-density-physics experiments

W. A. Stygar,[1] T. J. Awe,[1] J. E. Bailey,[1] N. L. Bennett,[2] E. W. Breden,[1] E. M. Campbell,[1,3]
R. E. Clark,[4] R. A. Cooper,[5] M. E. Cuneo,[1] J. B. Ennis,[6] D. L. Fehl,[1] T. C. Genoni,[4]
M. R. Gomez,[1] G. W. Greiser,[7] F. R. Gruner,[8] M. C. Herrmann,[9] B. T. Hutsel,[1] C. A. Jennings,[1]
D. O. Jobe,[10] B. M. Jones,[1] M. C. Jones,[1] P. A. Jones,[1] P. F. Knapp,[1] J. S. Lash,[1] K. R. LeChien,[11]
J. J. Leckbee,[1] R. J. Leeper,[12] S. A. Lewis,[1] F. W. Long,[1] D. J. Lucero,[1] E. A. Madrid,[4]
M. R. Martin,[1] M. K. Matzen,[1] M. G. Mazarakis,[1] R. D. McBride,[1] G. R. McKee,[1] C. L. Miller,[4]
J. K. Moore,[1] C. B. Mostrom,[4] T. D. Mulville,[1] K. J. Peterson,[1] J. L. Porter,[1] D. B. Reisman,[1]
G. A. Rochau,[1] G. E. Rochau,[1] D. V. Rose,[4] D. C. Rovang,[1] M. E. Savage,[1] M. E. Sceiford,[1]
P. F. Schmit,[1] R. F. Schneider,[11] J. Schwarz,[1] A. B. Sefkow,[1] D. B. Sinars,[1]
S. A. Slutz,[1] R. B. Spielman,[13] B. S. Stoltzfus,[1] C. Thoma,[4] R. A. Vesey,[1]
P. E. Wakeland,[1] D. R. Welch,[4] M. L. Wisher,[1] and J. R. Woodworth[1]

[1]*Sandia National Laboratories, Albuquerque, New Mexico 87185, USA*
[2]*National Security Technologies, Las Vegas, Nevada 89193, USA*
[3]*Laboratory for Laser Energetics, University of Rochester, Rochester, New York 14623, USA*
[4]*Voss Scientific, Albuquerque, New Mexico 87108, USA*
[5]*General Atomics, San Diego, California 92186, USA*
[6]*NWL Capacitor Division, Snow Hill, North Carolina 28580, USA*
[7]*CSI Technologies, Vista, California 92081, USA*
[8]*Kinetech Corporation, Cedar Crest, New Mexico 87008, USA*
[9]*Lawrence Livermore National Laboratory, Livermore, California 94550, USA*
[10]*Tech Source Consulting, Ashburn, Virginia 20148, USA*
[11]*National Nuclear Security Administration, Washington, DC 20585, USA*
[12]*Los Alamos National Laboratory, Los Alamos, New Mexico 87545, USA*
[13]*Idaho State University, Pocatello, Idaho 83209, USA*
(Received 8 April 2015; published 30 November 2015)

We have developed conceptual designs of two petawatt-class pulsed-power accelerators: Z 300 and Z 800. The designs are based on an accelerator architecture that is founded on two concepts: single-stage electrical-pulse compression and impedance matching [Phys. Rev. ST Accel. Beams **10**, 030401 (2007)]. The prime power source of each machine consists of 90 linear-transformer-driver (LTD) modules. Each module comprises LTD cavities connected electrically in series, each of which is powered by 5-GW LTD bricks connected electrically in parallel. (A brick comprises a single switch and two capacitors in series.) Six water-insulated radial-transmission-line impedance transformers transport the power generated by the modules to a six-level vacuum-insulator stack. The stack serves as the accelerator's water-vacuum interface. The stack is connected to six conical outer magnetically insulated vacuum transmission lines (MITLs), which are joined in parallel at a 10-cm radius by a triple-post-hole vacuum convolute. The convolute sums the electrical currents at the outputs of the six outer MITLs, and delivers the combined current to a single short inner MITL. The inner MITL transmits the combined current to the accelerator's physics-package load. Z 300 is 35 m in diameter and stores 48 MJ of electrical energy in its LTD capacitors. The accelerator generates 320 TW of electrical power at the output of the LTD system, and delivers 48 MA in 154 ns to a magnetized-liner inertial-fusion (MagLIF) target [Phys. Plasmas **17**, 056303 (2010)]. The peak electrical power at the MagLIF target is 870 TW, which is the highest power throughout the accelerator. Power amplification is accomplished by the centrally located vacuum section, which serves as an intermediate inductive-energy-storage device. The principal goal of Z 300 is to achieve thermonuclear ignition; i.e., a fusion yield that exceeds the energy transmitted by the accelerator to the liner. 2D magnetohydrodynamic (MHD) simulations suggest Z 300 will deliver 4.3 MJ to the liner, and achieve a yield on the order of 18 MJ. Z 800 is 52 m in diameter and stores 130 MJ. This accelerator generates 890 TW at the output of its LTD system, and delivers 65 MA in 113 ns to a MagLIF target. The peak electrical power at the MagLIF liner is 2500 TW. The principal goal of Z 800 is to achieve high-yield

thermonuclear fusion; i.e., a yield that exceeds the energy initially stored by the accelerator's capacitors. 2D MHD simulations suggest Z 800 will deliver 8.0 MJ to the liner, and achieve a yield on the order of 440 MJ. Z 300 and Z 800, or variations of these accelerators, will allow the international high-energy-density-physics community to conduct advanced inertial-confinement-fusion, radiation-physics, material-physics, and laboratory-astrophysics experiments over heretofore-inaccessible parameter regimes.

I. INTRODUCTION

Over the past five decades, more than one hundred major pulsed-power accelerators have been developed by the international scientific community. A number of new accelerators are under development, including the Thor [1], Primary Test Stand [2], and Baikal [3] machines, in the United States, China, and Russia, respectively.

Presently, the world's largest and most powerful pulsed-power accelerator is the refurbished Z machine, also referred to as ZR [4–16]. The ZR accelerator, which was completed in 2007, is located at Sandia National Laboratories in Albuquerque, New Mexico, USA. The ZR Facility conducts approximately 150 accelerator shots each year. These drive a wide variety of high-energy-density-physics (HEDP) experiments in support of the U.S. National Nuclear Security Administration's Stockpile Stewardship Program.

ZR represents the state of the art of conventional pulsed-power-accelerator technology. ZR stores 20 MJ of electrical energy at a Marx charge voltage of 85 kV, achieves peak electrical powers as high as 85 TW at the accelerator's water-vacuum interface, and delivers as much as 26 MA in a 100-ns electrical-power pulse to a physics-package load. The peak electrical power achieved at an idealized imploding liner is 200 TW. As much as 330 TW and 2.3 MJ are radiated by such loads in thermal x rays [17–27]. Experiments conducted on ZR (and its predecessor, the Z machine [20,28–39]) have, to date, motivated ~1000 peer-reviewed journal publications.

In this article, we propose to build upon the foundation established by Z and ZR: we propose to advance pulsed-power-driven HEDP experiments to a higher technological level by delivering substantially more current, energy, and power to a load than ZR does presently. The most direct and straightforward approach to next-generation experiments may simply be to design and build a larger version of the ZR machine. For the following reasons, we propose herein an alternate approach.

ZR includes 36 pulsed-power modules, each of which is driven by a Marx generator with an LC time constant $[(LC)^{1/2}]$ of 750 ns. (The quantities L and C are the series inductance and capacitance of each Marx, respectively.) Such a Marx generates an electrical power pulse with a temporal width on the order of 1 μs. Since HEDP experiments conducted on ZR require each module to generate a power pulse with a width on the order of 100 ns, each

module performs four stages of pulse compression. The compression hardware reduces the width of the pulse generated by each Marx by an order of magnitude.

Although the hardware successfully compresses the pulse, it introduces impedance mismatches, which cause multiple reflections of the pulse within the accelerator. The mismatches and reflections complicate the machine design, reduce the energy and power efficiencies of the accelerator, reduce accelerator-component lifetimes, and increase the effort required to maintain and operate the machine. In addition, the increased complexity inherent in the pulse-compression hardware increases the difficulty of conducting accurate circuit and electromagnetic simulations of an accelerator shot.

Thus we propose to base the designs of next-generation pulsed-power accelerators on an architecture founded on two fundamental concepts: single-stage electrical-pulse compression and impedance matching [40]. We propose that the LC time constant of the prime-power source of future machines be on the order of 100 ns, so that the electrical-power pulse generated by the source does not require additional compression. We also propose that, to the extent possible, the transmission lines that transport the power pulse from the prime-power source to the load be impedance matched throughout. This approach minimizes reflections within the accelerator and maximizes the efficiency at which electrical energy and power are delivered to the load.

In this article, we describe conceptual designs of two such accelerators: Z 300 and Z 800 [41]. These machines are petawatt-class accelerators that generate a 100-ns electrical power pulse at twice the energy efficiency of ZR. The principal goal of Z 300 is to achieve thermonuclear ignition; i.e., a fusion yield that exceeds the energy transmitted by the accelerator to a target. The principal goal of Z 800 is to achieve high-yield thermonuclear fusion; i.e., a yield that exceeds the energy initially stored by the accelerator's capacitors. These machines, or variations of them, will allow the international scientific community to conduct advanced inertial-confinement-fusion, radiation-physics, material-physics, and laboratory-astrophysics experiments over heretofore-inaccessible parameter regimes.

The proposed Z-300 and Z-800 accelerators are powered by linear-transformer-driver (LTD) modules [40–57]. An LTD module is a type of induction voltage adder (IVA) [58]. An IVA consists of several induction cavities

connected electrically in series. In a conventional IVA, each cavity is driven by electrical-pulse generators located *outside* the cavity. In an LTD, each cavity is driven by generators *within* the cavity.

The designs of Z 300 and Z 800 are based on the LTD-powered accelerator architecture outlined by Ref. [40]. The designs assume use of a recently developed 5-GW LTD brick [59]. Each brick includes two 100-kV 80-nF capacitors connected electrically in series with a single 200-kV field-distortion gas switch. The 5-GW brick generates twice the electrical power of the first-generation LTD brick [40,42–55]. The new brick reduces by a factor of 2 the volume required by an LTD module to generate a given peak electrical power, thereby substantially reducing the size of an LTD-powered accelerator.

Z 300's LTD system is designed to generate a peak electrical power as high as 320 TW. The conceptual design of Z 300 is outlined by Sec. II. This is a *point* design; no attempt has yet been made to vary the electrical parameters and geometry of the configuration to develop an *optimized* design; i.e., one that maximizes the performance of the accelerator for a given cost. We have developed two circuit models of Z 300: one assumes this machine is coupled to a magnetized-liner inertial-fusion (MagLIF) target [60–69]; the other, a dynamic hohlraum [70–75]. The models are described by Secs. III and IV; Sec. V summarizes the corresponding model predictions.

Z 800 is a larger version of Z 300, and is designed to generate a peak electrical power as high as 890 TW at the output of its LTD system. The conceptual design of Z 800, which is also a point design, is outlined by Sec. VI. MagLIF and dynamic-hohlraum circuit models of Z 800 are described by Secs. VII and VIII; model predictions are summarized by Sec. IX.

Given the cost of an accelerator such as Z 300 or Z 800, it is critical that the accelerator deliver—as efficiently as possible—energy stored in its capacitors to the load. Section X proposes a definition of the energy efficiency of a coupled accelerator-load system. Section XI discusses how the efficiency of the Z-300 and Z-800 systems might be increased.

Suggestions for future work are presented by Sec. XII. Auxiliary information is included in five Appendices.

To maximize the efficiency of an accelerator such as Z 300 or Z 800 it is essential to minimize the fractional current loss within the accelerator's stack-MITL system. Appendices A and B outline a physics model of such current loss, and describe an approach to limiting the loss to acceptable levels. The physics model is motivated in part by fully relativistic, full electromagnetic 2D and 3D particle-in-cell (PIC) simulations [5,6,12,31,76–79]. The approach to minimizing the loss is based on that used to design the successful stack-MITL system of Z [32,33,38].

It is clear that a complete understanding of the performance of an accelerator that generates on the order of a petawatt of peak electrical power in a 100-ns pulse requires detailed and accurate numerical simulations. Nevertheless, *approximate* analytic scaling relations provide meaningful insight into the operation of such a machine. Scaling relations applicable to both Z 300 and Z 800 are developed in Appendix C.

Comparing results of circuit simulations of different accelerator-load systems is complicated by the fact that such systems, in general, generate load-current time histories that are mathematically dissimilar. Consequently, two systems can achieve the same peak load current but deliver different energies to the load; two systems can achieve the same load-implosion time but deliver different final load-implosion velocities. To facilitate comparison of the results of such simulations, we define in Appendix D *effective* values of the peak load current and load-implosion time for MagLIF and dynamic-hohlraum loads.

The conceptual designs of Z 300 and Z 800 presented in this article are based on the LTD-powered accelerator architecture outlined by Ref. [40]. This reference also describes a Marx-generator-powered machine. As discussed by Appendix E, we choose to base the designs of Z 300 and Z 800 on the LTD-powered option in part because this design offers significant safety and environmental benefits.

Numbered equations are in SI units throughout.

II. CONCEPTUAL DESIGN OF Z 300

A cross-sectional view of a three-dimensional model of Z 300 is presented by Fig. 1. As indicated by the figure, Z 300 has four principal components: a system of 90 identical LTD modules connected electrically in parallel, six parallel water-insulated radial-transmission-line impedance transformers, a six-level vacuum insulator stack that serves as the accelerator's water-vacuum interface, and a system of vacuum transmission lines that delivers the electrical power generated by the accelerator to a physics load. The machine is 35 m in diameter overall.

The LTD modules serve as the prime power source of Z 300. Thirty modules are located and azimuthally distributed in each of three levels. As indicated by Fig. 2, each module comprises 33 identical LTD cavities connected electrically in series; hence Z 300 is powered by 2970 cavities altogether. Each of the 90 LTD modules is 2 m in diameter and 7.26 m in length.

Each module drives an internal water-insulated coaxial transmission line, the inner conductor of which serves as the cathode. To maximize the peak electrical power at the output of a module, the internal line must have an impedance profile that increases in a linear stepwise manner from the upstream to the downstream end of the module, as suggested by Fig. 3 of [47]. Such a profile can be achieved with a stepped cathode. However, 2D electromagnetic simulations demonstrate that a right-circular conical cathode (as illustrated by Figs. 1 and 2) that
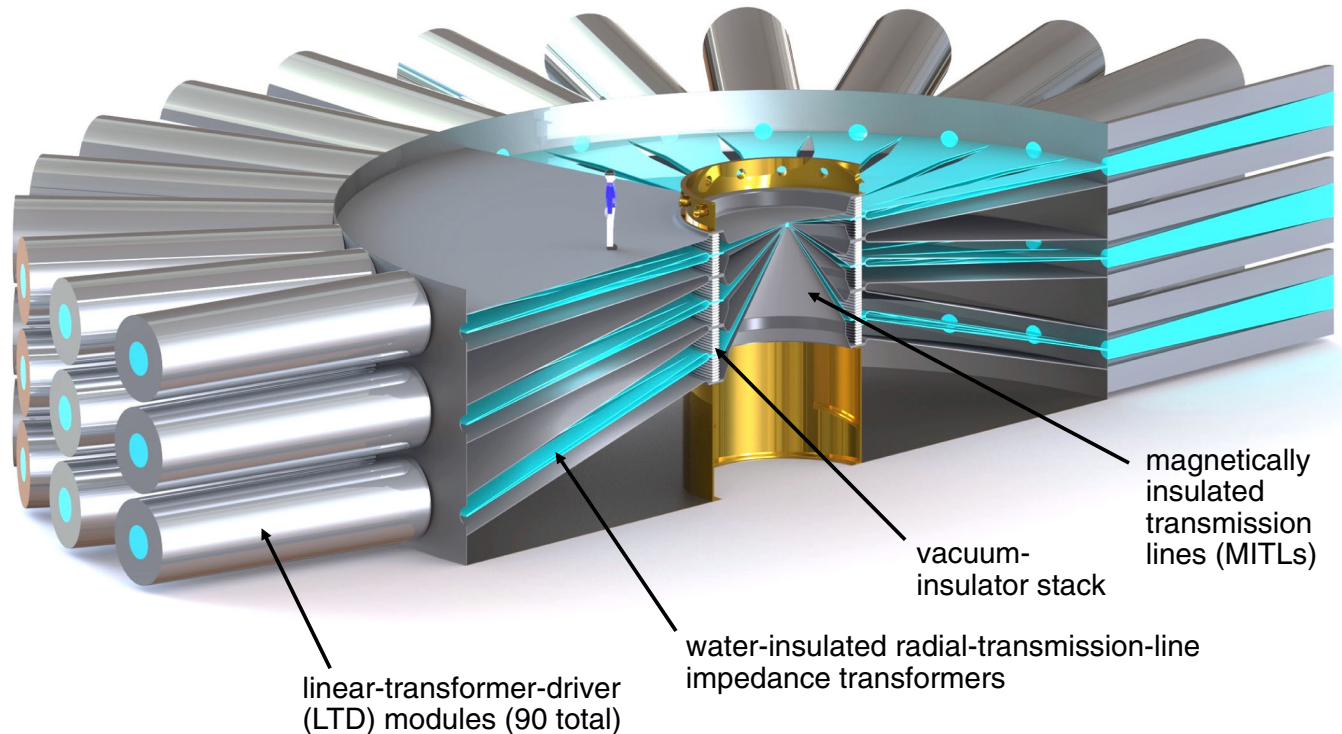
FIG. 1.   Cross-sectional view of a three-dimensional model of the Z-300 accelerator. The model includes a person standing on the uppermost water-section electrode, near the centrally located vacuum section. The outer diameter of Z 300 is 35 m.

approximates the optimized stepped geometry achieves 98% of the output power delivered by an optimized design [80].

Figure 3 is a cross-sectional view of a single LTD cavity. Each cavity is a right-circular annulus with an outer diameter of 2 m, an inner diameter of 0.8 m, and a length of 0.22 m. Each is driven by 20 identical LTD bricks connected electrically in parallel and distributed azimuthally within the cavity; hence Z 300 is powered by 59,400 bricks altogether. Each brick consists of two 80-nF capacitors connected in series with a single (normally open) 200-kV field-distortion gas switch.

The operation of a single LTD cavity can be inferred from Fig. 3. Before the switches are triggered, the capacitors are DC charged in a balanced $+100$ kV, -100 kV manner; the cavity wall serves as a common ground. Thus the total potential difference across each switch is 200 kV [81]. After the switches close, a potential difference of ~ 100 kV appears across the cavity's output gap. Hence each brick can be considered as a single two-stage Marx generator [81].

The ferromagnetic cores indicated by Fig. 3 prevent most of the current generated by the cavity from flowing along its internal walls; hence most of the current is delivered to the output gap. We assume the cores are fabricated from 23-μm-thick Metglas 2605CO tape. (Other core materials, such as Hitachi FT-3M, could also be used.) The total cross-sectional area of the cores within a single cavity is 77 cm^2;

70% of the core volume consists of the Metglas alloy itself. The total value of the volt-second product of the cores within a single cavity is 16 mV-s.

As discussed above, Z 300 is driven by 2970 LTD cavities, which altogether contain 59,400 LTD bricks. Each of the accelerator's 59,400 switches could be triggered by a 100-kV pulse delivered by a 200-ohm transmission line. Hence the peak electrical power required to trigger all the switches is 3 TW, which is a small fraction of the accelerator's total power.

The vertical cylindrical wall that separates the LTD modules from the Z-300 water section is located at a radius of 10.3 m. Each of the three LTD-module levels drives two water-insulated radial-transmission-line impedance transformers; i.e., a triplate. The six transformers are approximately horizontal and electrically in parallel. At a radius of 10.3 m, the anode-cathode (AK) gap of each of the six transformers is 41 cm; at a radius of 2.59 m, the AK gap is 38 cm.

The transformers transmit the power generated by the LTD modules to a centrally located vacuum section, illustrated by Fig. 4. As indicated by the figure, this section includes a six-level vacuum-insulator stack and a six-level system of conical outer magnetically insulated transmission lines.

This center-section design is based on the successful stack-MITL concept developed by McDaniel, Sincerny, Spielman, Corcoran, and colleagues for the Proto-II, Double-EAGLE, and Saturn accelerators [82–89]. The
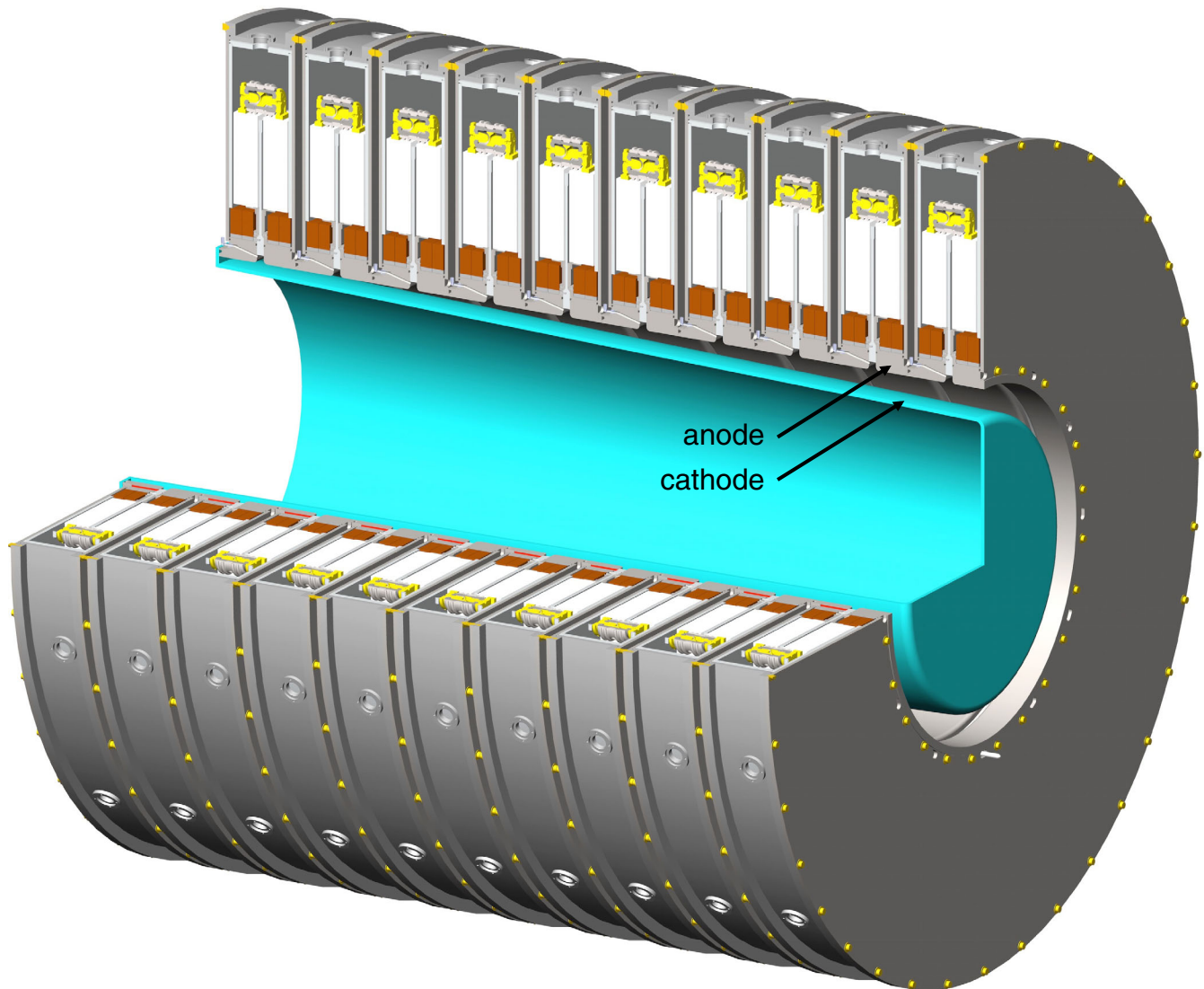
FIG. 2.   Cross-sectional view of a three-dimensional model of a ten-cavity 2-m-diameter LTD module. The anode and cathode are the electrodes of the module's internal water-insulated coaxial transmission line. Each Z-300 module includes 33 such cavities.

concept was subsequently applied to the designs of the stack-MITL systems of the Z [20,28–39] and ZR [4–16] machines. The Proto–II stack-MITL system delivered as much as ∼5 MA to a physics load; the Saturn system (which is still in operation) delivers ∼8 MA; the Z accelerator delivered 22 MA; the ZR accelerator delivers 26 MA.

We have selected the stack-MITL concept described by Refs. [4–7,10,12,16,20,28–35,37–39,76–79,82–89] for use on Z 300 because this design has been successfully operated on thousands of shots at load currents ranging from 5 to 26 MA. The design was used on Saturn to achieve 75 TW of x-ray power radiated by a wire-array z-pinch load [17,19]; on Z to achieve 280 TW [22]; and on ZR to achieve 330 TW [27]. The design has also enabled accelerator operation at the rate of a shot per day on Saturn, Z, and ZR. To date, no other stack-MITL concept has

demonstrated the electrical, mechanical, x-ray-power, and operational perfomance of the design described by Refs. [4–7,10,12,16,20,28–35,37–39,76–79,82–89].

The outer radius of Z 300's six-level insulator stack (illustrated by Figs. 1 and 4) is 2.39 m. As indicated by Figs. 1 and 4, there are six stacks altogether, one for each of the MITL system's six levels. As indicated by Fig. 4, the six-level stack includes seven horizontal electrodes, four of which are anodes, and three, cathodes. The gap between the anode and cathode electrodes on the water side of each of the top two insulator stacks is 46 cm. Hence the short water-insulated radial transmission line that extends from a radius of 2.59 to 2.39 m has an AK gap that increases from 38 to 46 cm, respectively. We refer to this short transmission line as a water flare. There are six water flares altogether, one for each stack level; the flares are illustrated by Figs. 4 and 5.
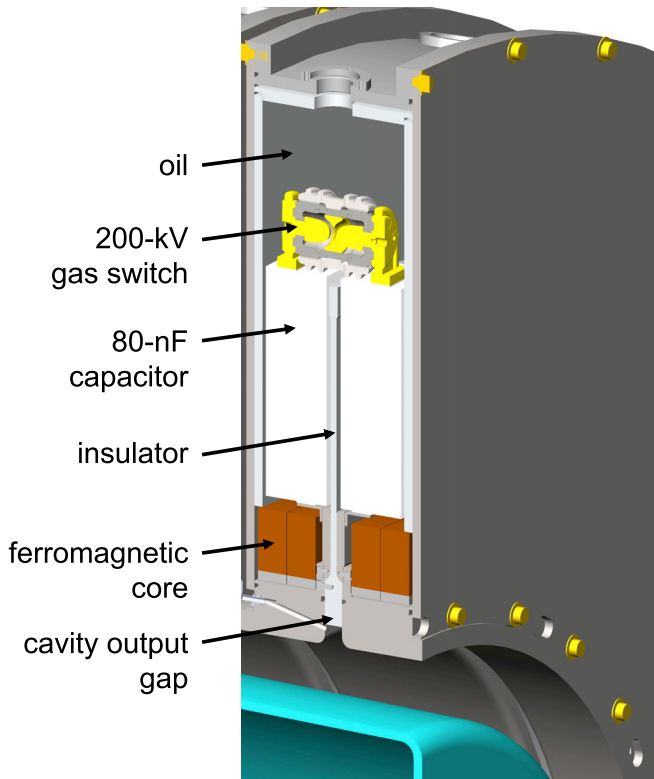
FIG. 3. Cross-sectional view of a single 2-m-diameter Z-300 LTD cavity. The upper terminal of one of the two capacitors is charged to +100 kV; the upper terminal of the other is charged to −100 kV. The lower terminal of each capacitor is initially at ground potential. When the capacitors are fully charged, the potential difference across the switch is 200 kV. After the switch closes, the peak voltage across the cavity's output gap reaches ∼100 kV. The ferromagnetic cores prevent most of the LTD's current from flowing along the inner walls of the cavity, which allows most of the current to be delivered to the output gap.

Each of the two uppermost stacks includes seven 5.72-cm-thick Rexolite-insulator rings and six 0.95-cm-thick anodized-aluminum grading rings. The middle two stacks include eight insulator and seven grading rings; the lower two, nine insulator and eight grading rings. To increase their flashover strength, the stacks use anode plugs [90,91], which are not included in Figs. 4 and 5.

As indicated by Figs. 4 and 5, six vacuum flares connect the six stacks to six conical outer magnetically insulated vacuum transmission lines (MITLs). The outer MITLs extend radially inward to a radius of 14 cm, at which the MITLs connect to a triple-post-hole vacuum convolute (which is not shown in Fig. 4) [5,6,12,38,76–79,82–89]. The posts of the convolute are located at a 10-cm radius. The convolute connects the six MITLs in parallel, combines the currents at the outputs of the MITLs, and delivers the combined current to a single short inner MITL. The convolute connects to the inner MITL at a 7-cm radius. The inner MITL transmits the combined current to the accelerator's physics-package load. (We refer to the six

MITLs located upstream of the convolute as the outer MITLs, and the single short MITL located downstream as the inner MITL.)

Z 300 will drive a wide variety of experimental configurations, including MagLIF targets and dynamic hohlraums. The inner MITL that couples to a MagLIF load has a radial section followed by a coaxial section, as illustrated by Fig. 6. The inner MITL that connects to a dynamic hohlraum has a similar design.

III. CIRCUIT MODELS OF Z 300

We have developed two circuit models of the Z-300 accelerator. The models were developed using the SCREAMER circuit code [92,93]. One model assumes Z 300 is coupled to a MagLIF target [60–69]; the other, a dynamic hohlraum [70–75]. Both circuit models are represented by Fig. 7. The circuit elements of this figure are described in this section.

The quantity C_s is the capacitance of Z-300's system of 90 LTD modules (which are electrically in parallel), and is given by the following expression:

$$C_s = \frac{n_b n_m}{n_c} C_b, \tag{1}$$

where

$$n_b = 20, \tag{2}$$

$$n_m = 90, \tag{3}$$

$$n_c = 33, \tag{4}$$

$$C_b = 40 \text{ nF}. \tag{5}$$

The quantity n_b is the total number of LTD bricks within a single LTD cavity, n_m is the total number of LTD modules, n_c is the total number of LTD cavities within a single LTD module, and C_b is the capacitance of a single brick (which includes two 80-nF capacitors connected in series).

We define V_s to be the initial charge voltage across the system of LTD modules:

$$V_s = n_c V_b, \tag{6}$$

$$V_b = 200 \text{ kV}, \tag{7}$$

where V_b is the initial charge voltage across a single LTD brick. The initial voltage is applied in a balanced manner, so that +100 kV appears across one of the brick's capacitors, −100 kV across the other, and 200 kV across the brick's switch [81]. The initial energy stored by the LTD capacitors E_s is one measure of the size of the accelerator:

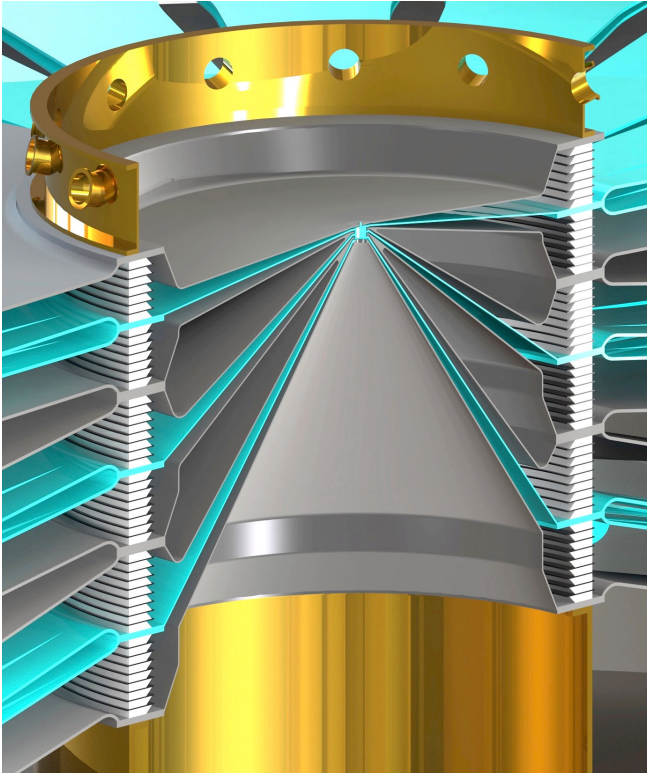$$E_s = \frac{1}{2} C_s V_s^2 = \frac{1}{2} n_t C_b V_b^2, \tag{8}$$

FIG. 4. Cross-sectional view of the centrally located vacuum section of Z 300. The section includes six water flares, six vacuum insulator stacks, six vacuum flares, and six conical outer MITLs. The six levels of this system are electrically in parallel. The outer radius of the stack is 2.39 m.
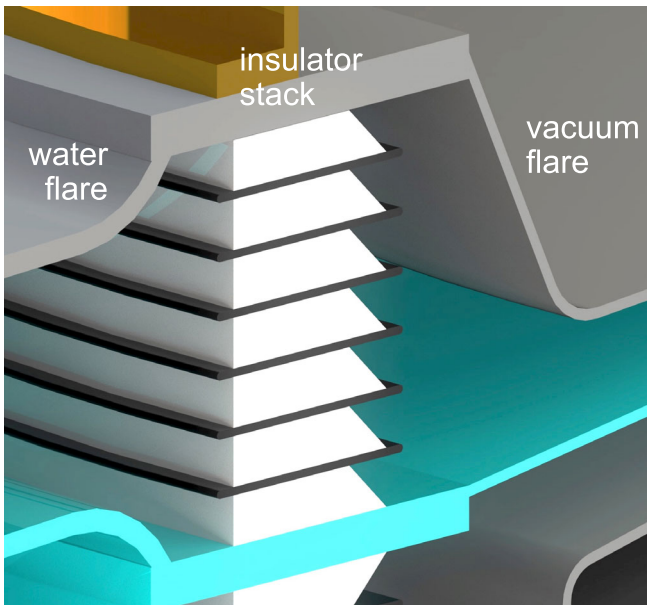

FIG. 5. Cross-sectional view of the water flare, insulator stack, and vacuum flare of the uppermost level of the six-level Z-300 insulator stack. The uppermost stack includes seven 5.72-cm-thick Rexolite-insulator rings and six 0.95-cm-thick anodized-aluminum grading rings.

$$n_t = n_b n_c n_m = 59,400, \qquad (9)$$

where n_t is the total number of LTD bricks in the machine.

We assume the series inductance and resistance of the system of LTD modules, L_s and R_s respectively, can be approximated as constants:

$$L_s = \frac{n_c}{n_b n_m} L_b, \qquad (10)$$

$$L_b = 160 \text{ nH}, \qquad (11)$$

$$R_s = \frac{n_c}{n_b n_m} R_b, \qquad (12)$$

$$R_b = 0.3 \ \Omega, \qquad (13)$$

where L_b and R_b are the series inductance and resistance of a single brick.

The brick inductance and resistance are functions of the spatially dependent electron, ion, and neutral-particle temperatures and densities of the current-carrying plasma channels within the brick's switch. Hence the inductance and resistance must be time dependent. However, over the 100-ns time interval of interest, the performance of a brick can be approximated with reasonable accuracy by using effective constant values for the inductance and resistance. Equations (11) and (13) give the assumed effective values.

The shunt resistance of the system of LTD cavities R_{shunt} is a function of the shunt impedance of a single LTD cavity. This impedance is the sum of several terms, the dominant of which is the effective resistance of the Metglas cores located within the cavity, R_{cores}. This resistance is time dependent [54]:

$$R_{\text{cores}}(t) = \frac{2S(\mu\mu_0\rho_{\text{cores}})^{1/2}}{\pi^{3/2} r_{\text{cores}} \delta t^{1/2}}, \qquad (14)$$

where

$$S = 5.4 \times 10^{-3} \text{ m}^2, \qquad (15)$$

$$\mu \sim 1000, \qquad (16)$$

$$\mu_0 \equiv 4\pi \times 10^{-7}, \qquad (17)$$

$$\rho_{\text{cores}} = 1.23 \times 10^{-6} \ \Omega\text{-m}, \qquad (18)$$

$$r_{\text{cores}} = 0.46 \text{ m}, \qquad (19)$$

$$\delta = 2.3 \times 10^{-5} \text{ m}. \qquad (20)$$

The quantity S is the total cross-sectional area of the Metglas 2605CO material within a single cavity, μ is the effective relative permeability of the Metglas [94], μ_0 is the permeability of free space, ρ_{cores} is the electrical
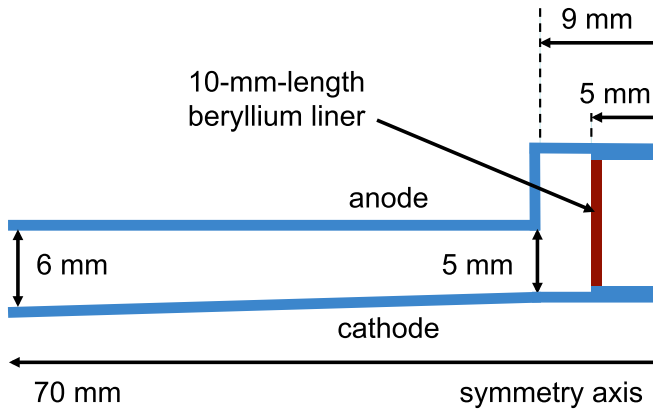
FIG. 6. Idealized representation of the inner MITL coupled to a MagLIF load.

resistivity of the Metglas, r_{cores} is the radius of the centroid of the core material, and δ is the thickness of the Metglas tape used to fabricate the cores. Equation (14) assumes the current pulse generated by the LTD cavity can be approximated as a linear ramp [54]; the time variable t assumes the ramp begins at $t = 0$. Equation (14) is consistent with results presented by Ref. [57], and gives resistances comparable to those given by Ref. [55].

The relative permeability μ is, of course, not constant as suggested by Eq. (16), but is instead a function of the time-dependent magnetic field at the surface of the Metglas [94]. Fortunately, when R_{cores} is much greater than the impedance of the 20 parallel LTD bricks located within a single LTD cavity (which would be the case when the cavity is well designed), the current delivered to the physics load is

an insensitive function of R_{cores}, which itself is proportional to the square root of μ. Hence the load current is an insensitive function of μ. Consequently we make the simplifying assumption that both μ and R_{cores} can be approximated as constants, and use the value of R_{cores} at $t = 100$ ns to estimate R_{shunt}, the shunt resistance of the system of LTD modules:

$$R_{shunt} = \frac{n_c}{n_m} R_{cores}(t = 100 \text{ ns}). \tag{21}$$

The optimum output impedance of the system of LTD modules Z_s is given by Refs. [40,47]:

$$Z_s = Z_{s,\text{ideal}} \left(1 - 0.73 \frac{Z_{s,\text{ideal}}}{R_{shunt}} \right), \tag{22}$$

$$Z_{s,\text{ideal}} = 1.10 \sqrt{\frac{L_s}{C_s}} + 0.80 \, R_s. \tag{23}$$

We define the optimum impedance to be that which maximizes the peak forward-going power at the output of the modules. (The quantity $Z_{s,\text{ideal}}$ would be the optimum impedance if there were no current loss within the cavities; i.e., if R_{shunt} were infinite.) According to Eqs. (1)–(5) and (10)–(23),

$$Z_s = 0.044 \ \Omega. \tag{24}$$

To maximize the peak forward-going power delivered by the modules to the water-insulated radial-transmission-line
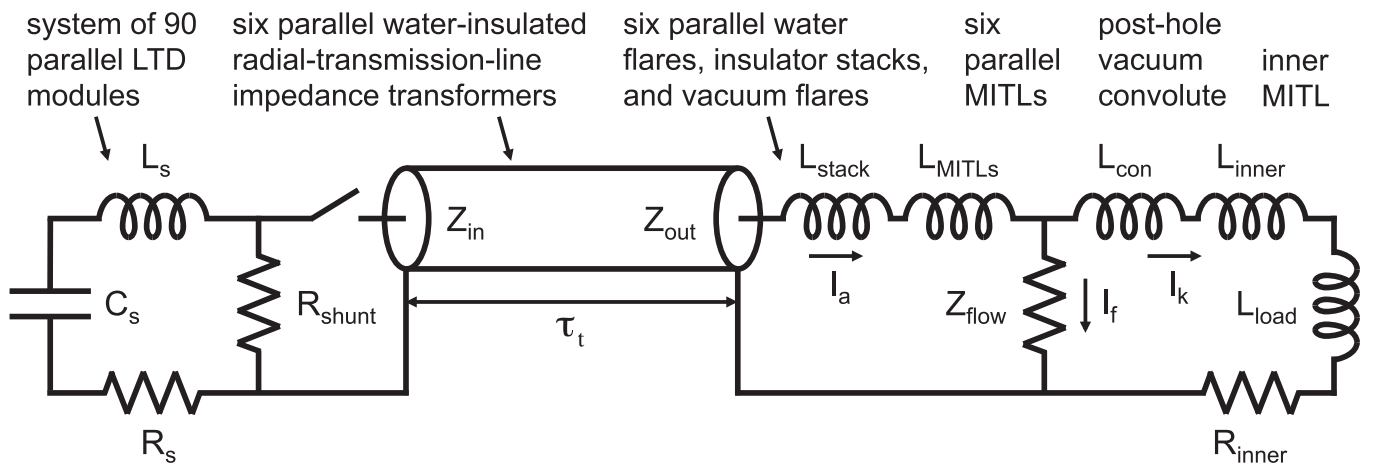

FIG. 7. Circuit model of the Z-300 and Z-800 accelerators. The quantities L_s, C_s, and R_s are the series inductance, capacitance, and resistance, respectively, of the system of 90 parallel LTD modules; R_{shunt} is the shunt resistance of the LTD system; Z_{in} and Z_{out} are the input and output impedances, respectively, of the system of six parallel transmission-line impedance transformers; L_{stack} is the total inductance of the water flares, insulator stacks, and vacuum flares; L_{MITLs} is the inductance of the six parallel MITLs; L_{con} is the inductance of the triple-post-hole vacuum convolute; L_{inner} is the inner-MITL inductance; L_{load} is the load inductance; and R_{inner} is a resistive circuit element that models energy loss to the inner-MITL electrodes. We define the quantity L_{load} so that $L_{load}(t = 0) = 0$. The Z_{flow} circuit element is used to model MITL-electron-flow current that is launched in the outer MITLs and lost to the anode surfaces of the convolute and inner MITL.

impedance transformers, we set the input impedance of the transformers Z_{in} equal to the output impedance of the LTD system:

$$Z_{in} = Z_s. \qquad (25)$$

The total length of the transformers is 7.7 m. At frequencies of interest the dielectric constant of water is 80; therefore, the one-way transit time of the transformers is 230 ns:

$$\tau_t = 230 \text{ ns.} \qquad (26)$$

We assume that the impedance of the system of transformers increases exponentially over the system's length [40,95,96] from Z_{in} to Z_{out}, which is the impedance of the transformer system at its output. (Other impedance profiles may offer superior performance [96].) We also assume the resistivity of the water used to insulate the transformers is 3×10^4 Ω-m:

$$\rho_w = 3 \times 10^4 \ \Omega\text{-m.} \qquad (27)$$

The circuit elements used to account for the water resistivity are not represented in Fig. 7.

We use Eq. (C12) to obtain an initial estimate of the value of Z_{out} that maximizes the peak electrical power delivered by the transformer system to Z-300's centrally located inductive vacuum section (i.e., the center section). Using this estimate as an initial value, we determine through iterative circuit simulations that for the circuit illustrated by Fig. 7, the performance of Z 300 is optimized when

$$Z_{out} = 0.165 \ \Omega. \qquad (28)$$

We define L_{stack} to be the sum of three sets of inductances: those due to the six parallel water flares, six parallel individual insulator stacks, and six parallel vacuum flares:

$$L_{stack} = 4.14 \text{ nH.} \qquad (29)$$

We define L_{MITLs} to be the inductance of the system of six parallel vacuum MITLs:

$$L_{MITLs} = 5.97 \text{ nH.} \qquad (30)$$

Not all the current delivered to Z 300's insulator stack is delivered to the load. To estimate the current that is lost, the Z-300 circuit simulations use the current-loss model described by Ref. [38]. This model was used to design the stack-MITL system of Z [32,33,38]. Over the course of the 1765 shots that were conducted during the ten-year lifetime of Z, no modifications to Z's stack or MITL system were needed. The loss model is consistent, to within

experimental uncertainties, with power-flow measurements conducted on Z, as suggested by Tables VII, VIII, and IX and Figs. 6–10 of Ref. [38].

The loss model makes the simplifying and conservative assumption that all the electron-flow current launched in the outer MITLs is lost to the anode immediately upstream of the convolute [32,33,38]. According to Table II of Ref. [97], measured electron-flow currents for a variety of MITLs fall between the predictions of collisionless and collisional MITL models. The collisional model predicts a higher value of flow current [97]; hence the loss model assumes that the electron flow in the MITLs is fully collisional [38,97].

Fully relativistic, fully electromagnetic 2D and 3D PIC simulations are consistent with the current-loss model: the simulations conducted to date suggest that essentially all the electron-flow current launched in the outer MITLs is lost to the anode electrodes of the convolute and inner MITL [5,6,12,76–79]. (It should be noted that these simulations may have been conducted with insufficient spatial resolution. A higher-resolution capability is presently under development.)

The current-loss model also assumes that the water flares, insulator stacks, vacuum flares, outer MITLs, convolute, inner MITL, and load are designed and operated in such a manner that the loss described above is the dominant loss mechanism. A more complete discussion of current loss in the stack-MITL system is presented by Appendices A and B.

As indicated by Fig. 7, the current loss is calculated using a Z-flow circuit element [98–101], which is defined by the following equations:

$$V_{MITLs} = Z_{flow}(I_a{}^2 - I_k{}^2)^{1/2}, \qquad (31)$$

$$Z_{flow} = \frac{2}{3}(0.9 Z_{MITLs}), \qquad (32)$$

$$Z_{MITLs} = \frac{Z_{single \, MITL}}{n_{MITLs}}, \qquad (33)$$

$$Z_{single \, MITL} = 5 \ \Omega, \qquad (34)$$

$$n_{MITLs} = 6, \qquad (35)$$

$$I_{loss} = I_f \equiv I_a \text{-} I_k. \qquad (36)$$

The quantity V_{MITLs} is the voltage at the output of the outer-MITL system. Equation (31) is given by Refs. [98–101]. Equation (32) is obtained from Ref. [97]; the factor of 0.9 is included here to account for gap closure, as discussed below. The quantity I_a is the anode current of the outer-MITL system, which is the total current upstream of the Z_{flow} circuit element; I_k is the outer-MITL-system cathode current, which we assume is the total current downstream, and the current delivered to the load; Z_{MITLs} is the vacuum impedance of the system of outer MITLs;

$Z_{\text{single MITL}}$ is the vacuum impedance of a single MITL; n_{MITLs} is the number of MITLs in the outer-MITL system; I_{loss} is the current that flows through the Z_{flow} circuit element; and I_f is the electron-flow current of the outer-MITL system.

The factor of 0.9 in Eq. (32) is included to account for closure of the outer-MITL AK gaps during the electrical-power pulse. We assume that the smallest MITL gap upstream of the convolute (i.e., at a radius of 14 cm) is 1.17 cm, the effective gap-closure velocity is a constant 1.1 cm/μs [102], and the length of the power pulse is 100 ns. (Reference [38] assumes a 2.5 cm/μs gap-closure velocity. However, as indicated by Tables II and III of [38], the MITL-system design described in [38] is insensitive to the gap-closure velocity for velocities between 0 cm/μs and 2.5 cm/μs. This is because the system's MITLs have impedances that vary with radius, and the lowest-impedance regions of the MITLs have the largest AK gaps.) Recent experiments [102] and simulations [103] demonstrate that the expansion velocity of the cathode plasma in a MITL is not, in fact, constant, and instead decreases with time. For MITL gaps and time scales of interest, the results of Ref. [102] suggest that for the first 100 ns, the average gap-closure velocity is approximately 1.1 cm/μs.

As discussed above, Eq. (36) makes the simplifying and conservative assumption that all the electron-flow current launched in the outer MITLs flows through Z_{flow}; i.e., is lost to the anode at the Z_{flow} circuit element. The quantities V_{MITLs}, I_a, I_k, and I_{loss} are calculated in a self-consistent manner by SCREAMER [92,93].

The quantity L_{con} of Fig. 7 is the inductance of the triple-post-hole vacuum convolute. We estimate the inductance of such a convolute with posts located on a 10-cm radius to be approximately 2 nH:

$$L_{\text{con}} = 2 \text{ nH.} \tag{37}$$

The quantity L_{inner} is the inductance of the inner MITL. For the circuit model of Z 300 that drives a MagLIF load, we assume the inner-MITL dimensions given by Fig. 6. To simplify the discussion in Sec. IV, we define L_{inner} to be the initial inductance of the conductors illustrated by Fig. 6; i.e., the initial inductance of everything inside a 7-cm radius:

$$L_{\text{inner}} = 3.48 \text{ nH.} \tag{38}$$

The inner MITL assumed for the dynamic hohlraum has dimensions similar to those given by Fig. 6; the Z-300 circuit model that drives a dynamic hohlraum assumes

$$L_{\text{inner}} = 2.91 \text{ nH.} \tag{39}$$

The resistive circuit element R_{inner} of Fig. 7 accounts for energy loss to the inner-MITL electrodes, which are

operated at peak lineal current densities that reach 15 MA/cm. This resistance, which is time dependent, is calculated in a self-consistent manner by SCREAMER using Eq. (35) of Ref. [104]. This equation accounts for energy loss due to Ohmic heating of the inner-MITL electrodes, diffusion of magnetic field into the electrodes, $\mathbf{j} \times \mathbf{B}$ work on the electrodes, and the increase in the inner-MITL's vacuum inductance due to motion of the vacuum-electrode boundary [104]. The element L_{load} of Fig. 7 is the load inductance, and is also time dependent.

IV. CIRCUIT MODELS OF THE MAGLIF AND DYNAMIC-HOHLRAUM LOADS ASSUMED FOR Z 300

For both the MagLIF and dynamic-hohlraum loads, the circuit element L_{load} of Fig. 7 is modeled as the time-dependent inductance of an infinitely thin, perfectly stable imploding cylindrical liner that has infinite electrical conductivity. All the results presented in this article assume such an idealized liner.

The load is modeled as indicated by Fig. 8. To simplify the circuit model of the load, the boundary between the inner MITL and load is defined so that $L_{\text{load}}(t = 0) = 0$. This boundary is the cylindrical surface at the initial outer radius of the liner a_i, defined by Fig. 8.

As suggested by Fig. 8, the inductance of the load can be expressed as follows:

$$L_{\text{load}} = \frac{\mu_0 \ell}{2\pi} \ln \frac{a_i}{a}, \tag{40}$$

where ℓ is the length of the liner, a_i is the initial liner radius, and a is the liner radius at time t. Hence,
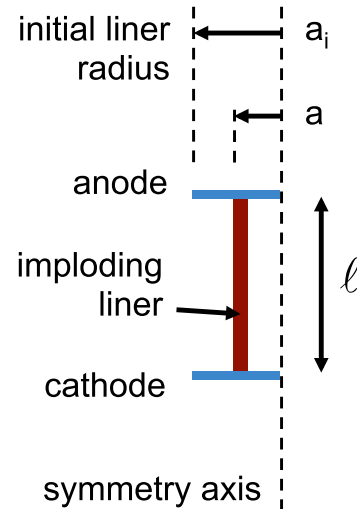

FIG. 8. Idealized representation of an imploding liner. The quantity a is the liner radius at time t, and ℓ is the length of the liner. For the MagLIF loads assumed in this article $a_i = 0.5$ cm and $\ell = 1.0$ cm [69].

$$\frac{dL_{\text{load}}}{dt} = \frac{-\mu_0 \ell v}{2\pi a}, \tag{41}$$

where $v = da/dt$ is the liner velocity at time t. (Since v is negative during the implosion, dL_{load}/dt is positive.)

We define V_{load} and P_{load} to be the voltage and power, respectively, at $r = a_i$:

$$V_{\text{load}} \equiv I_{\text{load}} \frac{dL_{\text{load}}}{dt} + L_{\text{load}} \frac{dI_{\text{load}}}{dt}, \tag{42}$$

$$P_{\text{load}} \equiv V_{\text{load}} I_{\text{load}} = I_{\text{load}}^2 \frac{dL_{\text{load}}}{dt} + L_{\text{load}} I_{\text{load}} \frac{dI_{\text{load}}}{dt}. \tag{43}$$

The load power can be expressed as the sum of kinetic and magnetic components, P_k and P_m:

$$P_{\text{load}} = P_k + P_m = P_k + \frac{d}{dt}\left(\frac{1}{2} L_{\text{load}} I_{\text{load}}^2\right), \tag{44}$$

where P_k is the power delivered to the kinetic energy of the liner, and P_m is the power delivered to the magnetic field within the radius a_i. Combining Eqs. (43) and (44) gives P_k:

$$P_k = \frac{1}{2} I_{\text{load}}^2 \frac{dL_{\text{load}}}{dt}. \tag{45}$$

We define E_{load} to be the total energy within the cylindrical volume bounded by $r = a_i$; this energy is the sum of kinetic and inductive components:

$$E_{\text{load}} \equiv \int_0^t P_{\text{load}} = K + \frac{1}{2} L_{\text{load}} I_{\text{load}}^2, \tag{46}$$

$$K \equiv \int_0^t P_k \, dt, \tag{47}$$

where K is the kinetic energy of the liner.

Equations (42) and (43) give the voltage and electrical power, respectively, at $r = a_i$. We define V_{liner} and P_{liner} to be the voltage and electrical power at the *instantaneous* liner radius a:

$$V_{\text{liner}} \equiv I_{\text{load}} \frac{dL_{\text{load}}}{dt}, \tag{48}$$

$$P_{\text{liner}} \equiv V_{\text{liner}} I_{\text{load}} = I_{\text{load}}^2 \frac{dL_{\text{load}}}{dt} = \frac{-\mu_0 \ell v}{2\pi a} I_{\text{load}}^2. \tag{49}$$

The quantities given by Eqs. (40)–(49) are calculated in a self-consistent manner by SCREAMER [92,93]. After peak load current $dI_{\text{load}}/dt < 0$; hence according to Eqs. (43) and (49), after peak load current, the liner power is greater than the load power:

$$P_{\text{liner}} > P_{\text{load}}. \tag{50}$$

It is clear that at any instant of time, P_{liner} is the sum of the power delivered to the kinetic energy of the liner and the power delivered to the creation of new magnetic field at $r = a$:

$$P_{\text{liner}} = P_k + P_m(r = a). \tag{51}$$

Combining Eqs. (45), (49), and (51), we find that at every instant of time, the power delivered to the liner's kinetic energy equals the power delivered to the creation of new magnetic field:

$$P_k = P_m(r = a) = \frac{1}{2} P_{\text{liner}}. \tag{52}$$

Because of this equivalence, the kinetic energy of the liner is (for much of the current pulse) approximately equal to the total magnetic energy within $r = a_i$. It is straightforward to show that for a current pulse that is constant in time, the kinetic energy of the liner is at all times exactly equal to the magnetic energy within $r = a_i$.

Assuming the load can be modeled as an infinitely thin and perfectly stable liner, the highest peak electrical power achieved throughout the entire accelerator is the peak value of P_{liner}. This value can exceed substantially the peak electrical power generated by the system of LTD modules, since the accelerator's centrally located vacuum section serves to amplify the power. As discussed above, the power pulse generated by the LTDs is delivered to the center section. Since the center section is inductive, it integrates a large fraction of the incoming power until peak load current is achieved. Consequently, the center section serves as an intermediate inductive-energy-storage device. After peak load current, when the load begins to implode much more rapidly than it does earlier in the current pulse, the center section delivers a fraction of its stored energy to the imploding load due to its rapidly increasing effective resistance. The characteristic time over which energy is delivered by the center section to the load is on the order of $L_{\text{center}}/(dL_{\text{load}}/dt)_f$, where L_{center} is the total inductance of the center section [as defined by Eq. (C4)] and $(dL_{\text{load}}/dt)_f$ is the effective liner resistance at the end of its implosion; i.e., the final effective liner resistance.

The circuit model of Z 300 that drives a MagLIF target assumes the load consists of a 444-mg beryllium liner with $a_i = 0.5$ cm and $\ell = 1$ cm [69].

The model of Z 300 that drives a dynamic hohlraum assumes this load consists of three components: a 2-cm-initial-radius 16.5-mg outer wire array; a 1-cm-initial-radius 8.26-mg inner array; and a 0.3-cm-radius foam cylinder located on axis [70–75]. We assume all the current initially flows in the outer array until it collides with the inner array at $r = 1$ cm. We make the simplifying assumption that the collision is perfectly inelastic, so that

after the collision, both arrays subsequently implode together. The axial length ℓ of the dynamic hohlraum is assumed to be 1.2 cm.

V. RESULTS OF Z-300 CIRCUIT SIMULATIONS

Results of SCREAMER simulations of Z-300 accelerator shots conducted with MagLIF and dynamic-hohlraum loads are summarized by Table I. The energy error of the simulations is 0.02%.

To minimize the probability of dielectric failure in Z 300's system of water-insulated radial impedance transformers, it is necessary for the transformers to satisfy everywhere the following relation [107,108]:

$$E_w \tau_w^{0.330} \leq 1.13 \times 10^5. \tag{53}$$

At a given location within the transformer system, the quantity E_w is the peak value in time of the electric field at the anode, and τ_w is the full temporal width of the voltage pulse at 63% of its peak value [107,108]. {Like the other numbered equations in this article, Eq. (53) is in SI units. Different units are used in Refs. [107,108].} Table I lists values of the quantity $E_w \tau_w^{0.330}$ as calculated by SCREAMER.

The probability that one or more of the six insulator stacks experience a total stack flashover on an accelerator shot is estimated using the statistical flashover model developed in Ref. [109]. As indicated by Table I, estimated flashover probabilities are less than 1%.

Figure 9(a) plots electrical powers at three locations within the accelerator, as calculated by the circuit simulation of Z 300 driving a MagLIF load. The stack voltage, stack current, and load current are plotted by Fig. 10(a). Other MagLIF-simulation results are summarized by Table I. This simulation finds that at a 10:1 liner-convergence ratio, 4.7 MJ of electrical energy is delivered to the MagLIF target. Significantly more accurate 2D magnetohydrodynamic (MHD) simulations indicate 4.3 MJ is delivered, and suggest the target will generate a thermonuclear yield on the order of 18 MJ [assuming the fuel is an optimized deuterium-tritium (DT) gas mixture] [69].

TABLE I.   Z-300 and Z-800 accelerator and load parameters. The second and fourth columns of the table assume a MagLIF load; the third and fifth assume the load is a dynamic hohlraum. The center-section inductance L_{center} is defined by Appendix C. The effective peak pinch current and implosion time are calculated as described by Appendix D. The final load-implosion velocity v_f, kinetic energy delivered to the load K_f, and accelerator efficiency η_a are—for the two simulations conducted with a MagLIF load—calculated when the load has achieved a 10:1 convergence ratio. For the two simulations conducted with a dynamic hohlraum, these quantities are calculated when the load has achieved a 6.7:1 convergence ratio. The fusion yields given in the last row are estimated using 2D MHD simulations [69]. The peak x-ray powers and total x-ray yields assume the dynamic hohlraum can be considered as an ablation-dominated wire-array z pinch [105,106], which suggests its radiated power and energy scale as indicated by Eqs. (54) and (55), respectively.

| Parameter	Z 300 (MagLIF)	Z 300 (dynamic hohlraum)	Z 800 (MagLIF)	Z 800 (dynamic hohlraum)
Outer accelerator diameter	35 m	35 m	52 m	52 m
Initial energy storage E_s	48 MJ	48 MJ	130 MJ	130 MJ
Peak power at the output of the LTD system	320 TW	320 TW	890 TW	890 TW
$E_w \tau_w^{0.330}$ at the output of the impedance transformers	1.11×10^5	1.11×10^5	1.09×10^5	1.08×10^5
Peak power at the input to the stack	260 TW	270 TW	740 TW	740 TW
Peak energy delivered to the stack	26 MJ	24 MJ	61 MJ	63 MJ
Center-section inductance L_{center}	20 nH	20 nH	24 nH	23 nH
Outer radius of the insulator stack	2.39 m	2.39 m	2.65 m	2.65 m
Peak voltage on the vacuum side of the stack	7.7 MV	7.6 MV	15 MV	14 MV
Probability that one or more of the six stacks flash during a shot	<1%	<1%	<1%	<1%
Effective peak load current I_{eff}	51 MA	47 MA	70 MA	70 MA
Peak value of the load current I_{load}	48 MA	45 MA	65 MA	67 MA
Load length ℓ	1 cm	1.2 cm	1 cm	1.2 cm
Initial load radius a_i	0.5 cm	2 cm	0.5 cm	2 cm
Total load mass	444 mg	25 mg	444 mg	56 mg
Effective load-implosion time $\tau_{i,eff}$	154 ns	120 ns	113 ns	120 ns
Final load-implosion velocity v_f	14 cm/μs	54 cm/μs	20 cm/μs	54 cm/μs
Kinetic energy delivered to the load K_f	4.7 MJ	3.6 MJ	8.7 MJ	8.3 MJ
Accelerator efficiency η_a	24%	21%	17%	17%
Peak value of P_{liner}	870 TW	700 TW	2500 TW	1500 TW
Estimated load performance	18-MJ fusion yield	510 TW, 4.7 MJ in thermal x rays	440-MJ fusion yield	950 TW, 11 MJ in thermal x rays
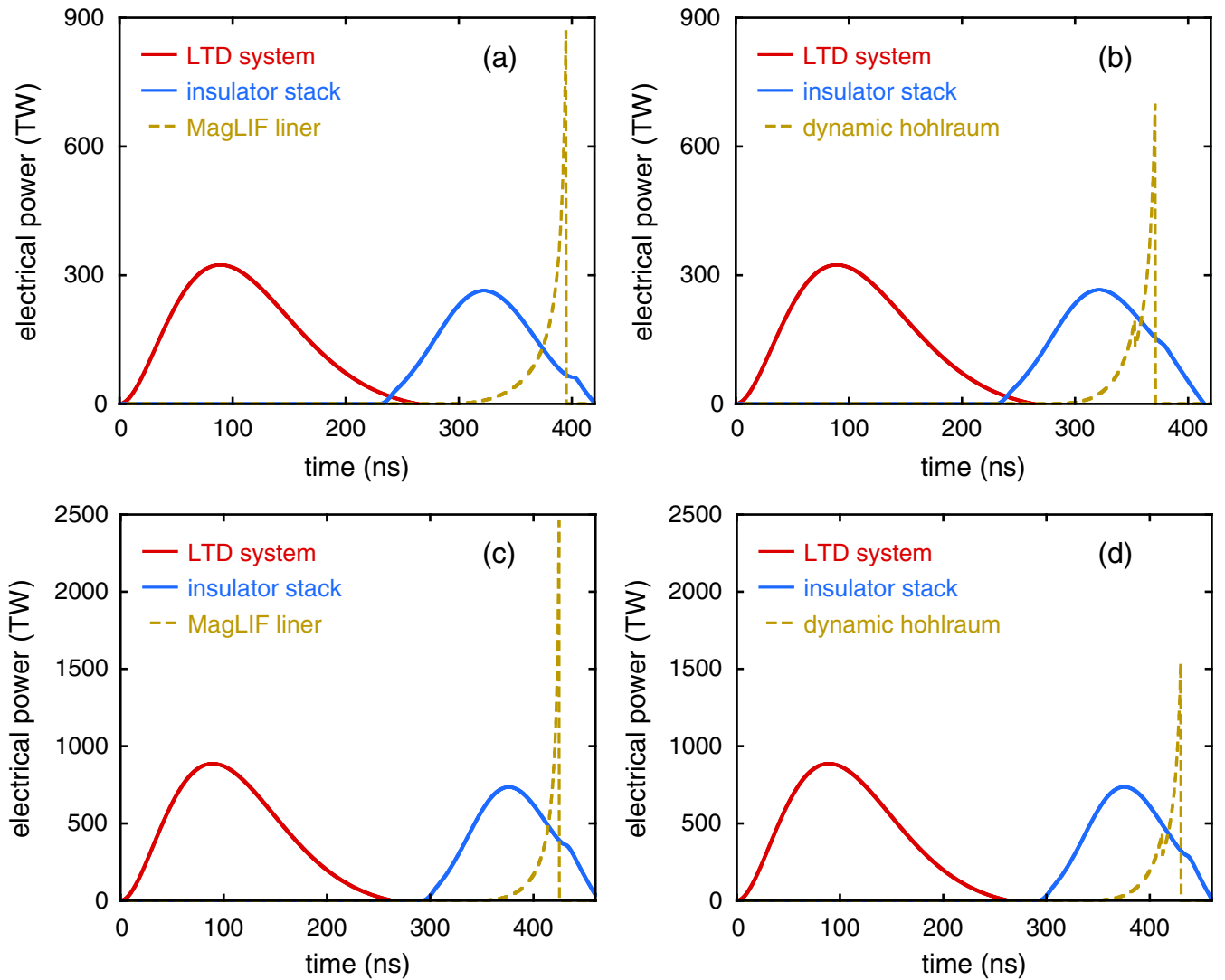
FIG. 9.   Simulated electrical-power time histories at the output of the LTD system, the input to the insulator stack, and the liner for (a) a Z-300 shot conducted with a MagLIF load; (b) a Z-300 shot conducted with a dynamic hohlraum; (c) a Z-800 shot conducted with a MagLIF load; and (d) a Z-800 shot conducted with a dynamic hohlraum.

Figure 9(b) plots electrical powers at three locations within the accelerator, as calculated by the circuit simulation of Z 300 driving a dynamic-hohlraum load. The stack voltage, stack current, and load current are plotted by Fig. 10(b). Other dynamic-hohlraum-simulation results are summarized by Table I.

The total mass per unit length of the two nested wire arrays of the dynamic hohlraum presently fielded on the ZR accelerator is 7.1 mg/cm [74]. The total mass per unit length of the two arrays of the dynamic hohlraum assumed for Z 300 is 21 mg/cm. According to Refs. [105,106], such wire-array z pinches are ablation dominated. Assuming the ZR and Z-300 dynamic hohlraums can be considered as ablation-dominated wire-array z pinches, the peak x-ray power P_r and total x-ray energy E_r radiated by such dynamic hohlraums scale approximately as follows [105,106]:

$$P_r \propto \left(\frac{I_{\text{eff}}}{\tau_{i,\text{eff}}}\right)^{3/2}, \tag{54}$$

$$E_r \propto I^2. \tag{55}$$

Assuming Eqs. (54) and (55), and the results presented by Ref. [74], we estimate that a dynamic hohlraum driven by Z 300 will radiate 510 TW and 4.7 MJ in thermal x rays. These results are included in Table I.

VI. CONCEPTUAL DESIGN OF Z 800

A cross-sectional view of a three-dimensional model of Z 800 is illustrated by Fig. 11. Z 800, which is 52 m in diameter, is a larger version of Z 300; hence the discussion in this section parallels that of Sec. II.
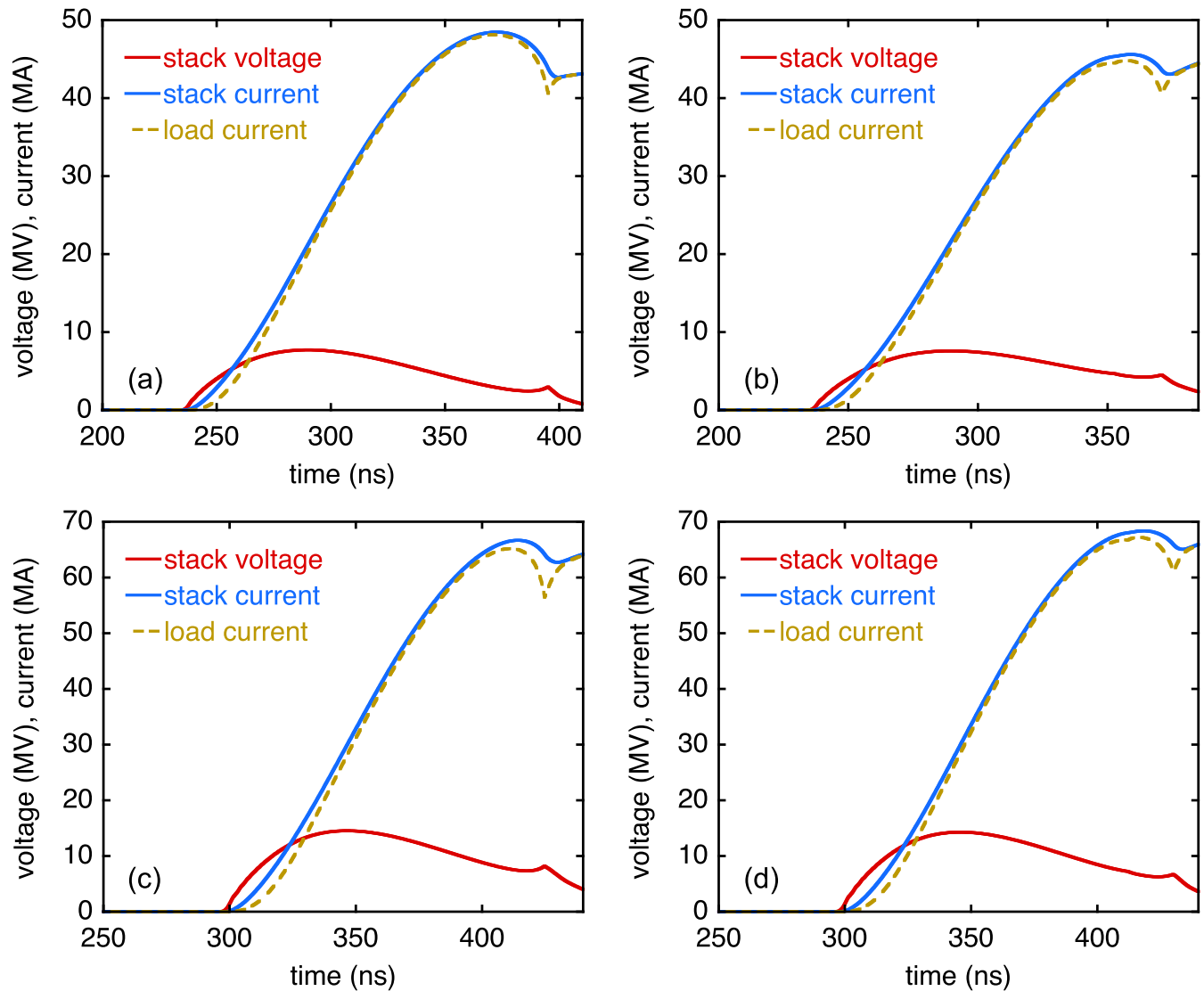
FIG. 10.   Simulated time histories of the voltage on the vacuum side of the insulator stack, current at the stack, and load current for (a) a Z-300 shot conducted with a MagLIF load; (b) a Z-300 shot conducted with a dynamic hohlraum; (c) a Z-800 shot conducted with a MagLIF load; and (d) a Z-800 shot conducted with a dynamic hohlraum.

Like Z 300, Z 800 is powered by 90 identical LTD modules connected electrically in parallel. Thirty modules are located and azimuthally distributed in each of three levels. Each module comprises 60 identical LTD cavities connected electrically in series; hence Z 800 is powered by 5400 cavities altogether. A single Z-800 module is a longer and larger-diameter version of the module represented by Fig. 2: each Z-800 module is 2.5 m in diameter and 13.2 m in length.

A cross-sectional view of a single Z-800 cavity is similar to that given by Fig. 3. Each Z-800 cavity is a right-circular annulus with an outer diameter of 2.5 m, an inner diameter of 1.3 m, and a length of 0.22 m. Each cavity is driven by 30 identical LTD bricks connected electrically in parallel and distributed azimuthally within the cavity; hence Z 800 is powered by 162,000 bricks altogether. Each brick is

identical to the 5-GW brick assumed for Z 300. The Metglas cores within the Z-800 cavities are identical to the cores used by Z 300, except the Z-800 cores are larger in diameter.

Each of the accelerator's 162,000 switches can be triggered by a 100–kV pulse delivered by a 200-ohm transmission line. Hence the peak electrical power required to trigger all the switches is 8 TW, which is a small fraction of the total accelerator power.

The vertical cylindrical wall that separates the LTD modules from the Z-800 water section is located at a radius of 12.7 m. Each of the three LTD-module levels drives two water-insulated radial-transmission-line imped-ance transformers; i.e., a triplate. At a radius of 12.7 m, the AK gap of each of the six transformers is 61 cm; at a radius of 2.85 m, the AK gap is 74 cm.
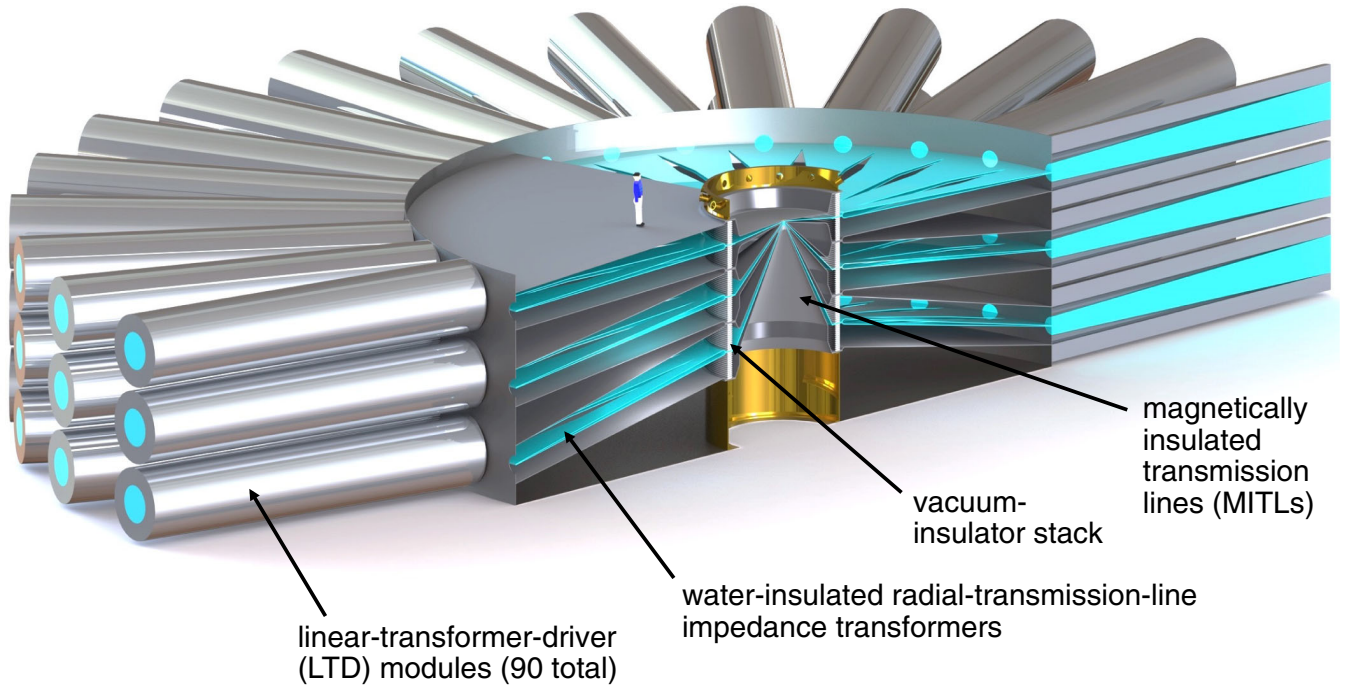
FIG. 11.   Cross-sectional view of a three-dimensional model of the Z-800 accelerator. The model includes a person standing on the uppermost water-section electrode, near the centrally located vacuum section. The outer diameter of Z 800 is 52 m.

The transformers transport the power generated by the LTD modules to a six-level vacuum-insulator stack. The outer radius of the stack, illustrated by Figs. 11 and 12, is 2.65 m. As indicated by these figures, the six-level stack includes seven horizontal electrodes, four of which are anodes, and three, cathodes. The gap between the anode and cathode electrodes on the water side of each of the top two insulator stacks is 79 cm. Each of the top two water flares that extend from a radius of 2.85 to 2.65 m has an AK gap that increases from 74 to 79 cm, respectively. As indicated by Figs. 11 and 12, there are six water flares altogether, one for each stack level.

Each of the two uppermost insulator stacks includes 12 5.72-cm-thick Rexolite-insulator rings and 11 0.95-cm-thick anodized-aluminum grading rings. Each of the middle two stacks includes 13 insulator and 12 grading rings; each of the lower two, 14 insulator and 13 grading rings. To increase their flashover strength, the stacks use anode plugs [90,91], which are not shown in Fig. 12.

As indicated by Fig. 12, six vacuum flares connect the six insulator stacks to six conical outer MITLs. The outer MITLs extend radially inward to a radius of 14 cm, at which the outer MITLs connect to a triple-post-hole vacuum convolute [5,6,12,38,76–79,82–89]. The posts are located at a 10-cm radius. The convolute connects the six MITLs in parallel, combines the currents at the outputs of the six MITLs, and delivers the combined current to a single short inner MITL. The convolute connects to the inner MITL at a 7-cm radius.

The inner MITL transmits the combined current to the accelerator's physics-package load. We assume Z 800 will use inner MITLs identical to those assumed for the Z 300 machine.

VII. CIRCUIT MODELS OF Z 800

We have developed two circuit models of the Z-800 accelerator. The models were developed using the SCREAMER circuit code [92,93]. One model assumes Z 800 drives a MagLIF target; the other, a dynamic hohlraum. Both models are represented by Fig. 7. Since the Z-300 and Z-800 circuit models have the same types of elements, we include in this section only equations that differ from those given in Sec. III.

For Z 800 we assume the following:

$$n_b = 30, \tag{56}$$

$$n_c = 60, \tag{57}$$

$$n_t = 162,000, \tag{58}$$

$$r_{\text{cores}} = 0.71 \text{ m}, \tag{59}$$

$$Z_s = 0.054 \ \Omega, \tag{60}$$

$$\tau_t = 292 \text{ ns}, \tag{61}$$

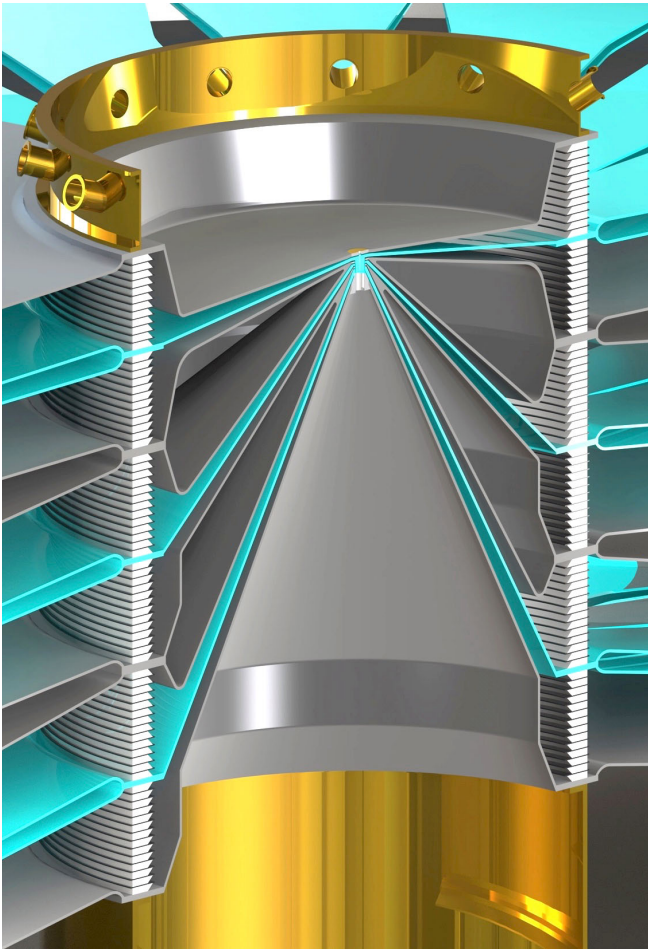$$Z_{\text{out}} = 0.29 \ \Omega, \tag{62}$$

FIG. 12. Cross-sectional view of the centrally located vacuum section of Z 800. This section includes six water flares, six vacuum insulator stacks, six vacuum flares, and six conical MITLs. The six levels of the system are electrically in parallel. The outer radius of the stack is 2.65 m.

$$L_{\text{stack}} = 6.28 \text{ nH.} \qquad (63)$$

$$L_{\text{MITLs}} = 7.22 \text{ nH.} \qquad (64)$$

VIII. CIRCUIT MODELS OF THE MAGLIF AND DYNAMIC-HOHLRAUM LOADS ASSUMED FOR Z 800

For both the MagLIF and dynamic-hohlraum loads, the circuit element L_{load} of Fig. 7 is modeled as described by Sec. IV. The MagLIF load assumed for Z 800 is identical to that assumed for Z 300. The dynamic hohlraum assumed for Z 800 is identical to that assumed for Z 300, except that for Z 800, the masses of the outer and inner arrays are 37.3 and 18.7 mg, respectively.

IX. RESULTS OF Z-800 CIRCUIT SIMULATIONS

Results of SCREAMER simulations of Z-800 accelerator shots conducted with MagLIF and dynamic-hohlraum

loads are summarized by Table I. The energy error of the simulations is 0.02%. The results parallel those obtained for Z 300, which are discussed by Sec. V.

Figure 9(c) plots electrical powers at three locations within the accelerator, as calculated by the simulation of Z 800 driving a MagLIF load. The stack voltage, stack current, and load current are plotted by Fig. 10(c). Other simulation results are summarized by Table I. This simulation finds that at a 10:1 liner-convergence ratio, 8.7 MJ of electrical energy is delivered to the MagLIF target. Significantly more accurate 2D MHD simulations indicate 8.0 MJ is delivered, and suggest the target will generate a thermonuclear yield on the order of 440 MJ (assuming the fuel is an optimized DT-gas mixture) [69]. This is substantially in excess of the 130 MJ initially stored by the Z-800 capacitors.

Figure 9(d) plots electrical powers at three locations within the accelerator, as calculated by the simulation of Z 800 driving a dynamic-hohlraum load. The stack voltage, stack current, and load current are plotted by Fig. 10(d). Other dynamic-hohlraum-simulation results are summarized by Table I.

Assuming (as suggested by Sec. V) that the ZR and Z-800 dynamic hohlraums can be considered as ablation-dominated wire-array z pinches, the peak x-ray power P_r and total x-ray energy E_r radiated by such dynamic hohlraums scale approximately as indicated by Eqs. (54) and (55), respectively. Assuming these equations and the results presented in Ref. [74], we estimate that a dynamic hohlraum driven by Z 800 will radiate 950 TW and 11 MJ in thermal x rays. These estimates are included in Table I.

X. ACCELERATOR ENERGY EFFICIENCY

The energy efficiency of a coupled accelerator-load system η_a is a function of time. We consider here the efficiency at the time at which the load has imploded to an arbitrarily specified final radius a_f, and define the efficiency as follows:

$$\eta_a \equiv \frac{K_f + 0.5(L_{\text{inner}} + L_{\text{load},f})I_f^2}{E_s}. \qquad (65)$$

The quantity K_f is the final kinetic energy of the liner, $L_{\text{load},f}$ is the final load inductance, and I_f is the load current at the time the liner has reached its final radius.

When the Ohmic resistance of the liner during its implosion can be neglected, K_f is the total energy delivered by the accelerator to the liner by the time it has completed its implosion. The quantity $0.5(L_{\text{inner}} + L_{\text{load},f})I_f^2$ is an estimate of the additional energy that could be delivered to the load on the time scale of interest, after it has achieved its final radius. This magnetic-energy term is added since the simple model of the load outlined by Sec. IV is incapable of simulating complex mechanisms that transfer energy from

the magnetic field to the load, such as those discussed in Refs. [17–26].

For the MagLIF load we arbitrarily assume that the liner convergence ratio is 10∶1. Hence we assume the final liner radius is 0.05 cm for both Z 300 and Z 800. For the dynamic hohlraum, we assume (for both machines) that the initial radius of the dynamic-hohlraum's outer wire array is 2 cm. The outer radius of the dynamic hohlraum's centrally located foam target is 0.3 cm. Hence for the dynamic hohlraum we assume the liner convergence ratio is 6.7∶1.

Estimates of the accelerator efficiency η_a for both Z 300 and Z 800 are included in Table I.

XI. ACCELERATOR-DESIGN CONSIDERATIONS

Maximizing the energy efficiency of the coupled accelerator-load system is one of the principal goals of an accelerator-design effort. In this section we discuss how the Z-300 and Z-800 accelerators might be made more efficient.

It is clear that the efficiencies of both machines could be increased by reducing the energy dissipated in resistances throughout the accelerator. More specifically, the efficiencies could be increased by increasing R_{shunt}, ρ_w, and Z_{flow}, and reducing R_s and R_{inner}.

The efficiencies of both machines could be increased by reducing the rise time of the LTD current pulse. This would increase the efficiency by delivering a larger fraction of the energy stored by the accelerator to the load during the desired implosion time. However, a faster rise time would also increase the peak voltage at the vacuum insulator stack. If the higher stack voltage were to require an increase in the height of the stack, L_{center} [defined by Eq. (C4)] would increase. An increase in L_{center} would counter this increased efficiency by decreasing the peak load current as indicated by Eqs. (C16) and (C22).

Alternatively, one could increase the time required for the load to implode by increasing its mass. However, this would decrease the load's final implosion velocity, which might compromise load performance. One could instead maintain the final implosion velocity by increasing the initial radius of the load while keeping its mass constant. This approach, which would increase the liner aspect ratio, might compromise load performance by increasing growth of implosion instabilities [17–26].

The efficiencies of Z 300 and Z 800 could be increased by improved impedance matching. For example, as suggested by Eq. (C8), the impedance transformers could be made more efficient by reducing $Z_{\text{out}}/Z_{\text{in}}$, the ratio of the impedance at the output of the transformers to that at the input. Since $Z_{\text{in}} = Z_s$ [Eq. (25)], this could be accomplished by increasing the LTD output impedance Z_s. This impedance could be increased by keeping the total number of LTD cavities constant, and rearranging the cavities into a fewer number of higher-impedance higher-voltage LTD modules. However, this would require longer and possibly larger-diameter modules, which would increase module fabrication and operational difficulties. This may also increase the outer diameter of the machine.

The impedance transformers could also be made more efficient by reducing the effective impedance of the accelerator's center section. This could be accomplished by reducing L_{center}, which would reduce Z_{out} as indicated by Eqs. (C12) and (C18) and hence reduce the transformer-impedance ratio $Z_{\text{out}}/Z_{\text{in}}$. Of course, reducing L_{center} would also directly increase the peak load current, as suggested by Eqs. (C16) and (C22).

The efficiency of the transformer system could be increased by increasing τ_t; however, this would require either increasing the outer diameter of the accelerator or using a liquid insulator with a dielectric constant greater than that of water. Increasing the accelerator diameter would increase the cost of the building within which the accelerator resides; use of a higher-dielectric-constant liquid insulator may create worker safety and environmental issues. The efficiency of the transformers may also be increased by using an impedance profile that is more efficient than the exponential function [96].

The efficiency of either Z 300 or Z 800 might be increased by changing the diameter of the insulator stack. No attempt has been made to calculate the accelerator efficiency as a function of stack diameter.

The designs of both accelerators assume the water-dielectric-breakdown relation developed by Refs. [107,108]. Increasing the dielectric strength of water, or using a liquid insulator with a higher-dielectric strength, would make it possible to use a lower value of Z_{out}. This would increase the efficiency of the impedance transformers, as suggested by Eq. (C8).

Developing an insulator stack with a dielectric-flashover strength greater than that of the insulator design described by Refs. [90,91] would make it possible to reduce the height and hence the inductance of the stack. This would reduce L_{center}, which would increase the peak load current as suggested by Eqs. (C16) and (C22).

Each machine could also be made more efficient by reducing current loss within the machine's stack-MITL system, which includes the insulator stacks, vacuum flares, outer MITLs, triple-post-hole vacuum convolute, inner MITL, and load. We discuss stack-MITL-system current loss in Appendices A and B.

XII. SUGGESTIONS FOR FUTURE WORK

The two conceptual designs outlined in this article suggest it is possible—with existing technology—to build an accelerator that delivers 45–70 MA in a 100-ns pulse to a physics-package load. Such a machine would revolutionize the field of high-energy-density physics. However, it is clear much work remains to be done.

The conceptual designs of Z 300 and Z 800 outlined herein are point designs; i.e., designs that are self-consistent but not optimized. The designs are intended to serve as a starting point for the development of an optimized final design of an advanced next-generation accelerator. The optimized design should address not only electrical performance but also safety, mechanical, operational, and cost considerations. Furthermore, the design must be compatible with requirements associated with the intended fusion yield.

We recommend that such an accelerator-optimization effort determine, for a given total number of LTD bricks n_t, the optimum number of bricks per LTD cavity, and the optimum number of cavities per LTD module. We also suggest such an effort optimize the outer and inner diameters of the LTD cavity, the cavity length, and the outer diameters of the accelerator and insulator stack.

In addition, this effort should determine the optimum number of accelerator levels. The conceptual designs of Z 300 and Z 800 each have six levels; i.e., each design includes six parallel transmission-line impedance transformers and a six-level stack-MITL system. However, as suggested by Ref. [40], it is not clear that the optimum number of levels is six; for example, eight may offer superior overall performance.

Furthermore, we recommend that the accelerator-development effort include the following activities: (1) development of a detailed transmission-line circuit model of the entire accelerator, from the LTDs to the load; (2) development of a 3D electromagnetic model of the entire accelerator; (3) development of a 3D mechanical model of the accelerator; (4) development of a 3D PIC model of the accelerator's coupled MITL-convolute-load system (this model would include, in a self-consistent manner, physics models of the formation and evolution of cathode and anode plasmas); (5) continued development of advanced switches, capacitors, ferromagnetic cores, capacitor-charge resistors, switch-trigger resistors, switch-trigger pulse generators, impedance-transformer designs, energy diverters, vacuum-insulator-stack designs, post-hole-convolute designs, and MITL-electrode-surface cleaning techniques; (6) design, fabrication, assembly, and commissioning of a full-scale 1/90th sector of the accelerator (the sector would include a full-scale LTD module, and a full-length transmission-line impedance transformer); (7) demonstration that the 1/90th sector meets all safety, electrical, mechanical, reliability, operational, and cost requirements; (8) development of 3D PIC models of the baseline MagLIF and dynamic-hohlraum loads that will be fielded on the new accelerator; (9) demonstration that the circuit, electromagnetic, mechanical, and PIC models listed above are predictive, which would indicate that the coupled accelerator-load system will perform as intended; and (10) development of an approach to manage the intended thermonuclear-fusion yields.

APPENDIX A: CURRENT LOSS WITHIN THE STACK-MITL SYSTEM UPSTREAM OF THE CONVOLUTE

In this Appendix, we outline a physics model of current loss within the Z-300 and Z-800 stack-MITL systems *upstream* of the triple-post-hole vacuum convolute, and discuss how this loss can be minimized. Current loss *within* the convolute and inner MITL is addressed by Appendix B.

The centrally located vacuum sections of the Z-300 and Z-800 accelerators are illustrated by Figs. 4 and 12, respectively. As indicated by Secs. II and VI, the designs of these center sections are based on the successful stack-MITL-system concept described by Refs. [4–7,10,12,16,20,28–35,37–39,76–79,82–89].

The Z-300 and Z-800 stack-MITL systems are six-level versions of the four-level systems discussed in [4–7,10,12,16,20,28–35,37–39,76–79,82–89]. Each of the six levels comprises a water flare, insulator stack, vacuum flare, and outer MITL. Each stack serves as the water-vacuum interface. The six levels are electrically in parallel. At a radius of 14 cm, the outer MITLs connect to a triple-post-hole vacuum convolute. The posts are located at a 10-cm radius. At a radius of 7 cm, the convolute connects to an inner MITL, which delivers the output current of the convolute to the load.

Several mechanisms can lead to current loss within such a system. Current can be lost along the plastic-vacuum interface of an insulator stack due to dielectric flashover [109]. Current can also be lost at the transition from a

vacuum flare to an outer MITL; such loss is referred to as MITL-injection loss [110]. In addition, current can be lost within an outer MITL (even after magnetic insulation is nominally established) due to electron leakage across the MITL's AK gap [97]; positive-ion emission from the MITL's anode electrode [111]; and negative-ion emission from the MITL's cathode [112,113].

Table II lists current-loss measurements that were performed on several Z-accelerator shots. The loss was measured within the Z stack-MITL system between $r = 165$ cm and $r = 80$ cm. The current measurements at $r = 165$ cm listed in the table were conducted immediately upstream of Z's plastic-vacuum interface, which was located at $r = 160$ cm. Each Z vacuum flare connected to an outer MITL at a radius of ~130 cm. Each outer MITL extended from $r \sim 130$ cm to $r = 10$ cm. Each outer MITL connected to Z's double-post-hole vacuum convolute at a radius of 10 cm; the convolute posts were located at a 7.62-cm radius.

The table demonstrates that insulator-stack, MITL-injection, electron-leakage, positive-ion, and negative-ion current loss can be neglected for a well-designed stack-MITL system, one based on the stack-MITL concept described by Refs. [4–7,10,12,16,20,28–35,37–39, 76–79,82–89]. According to Table II, the measured values of the total current loss between $r = 165$ cm and $r = 80$ cm are less than experimental uncertainties. The measurements are consistent with transmission-line-circuit [32,33,38] and 2D and 3D particle-in-cell (PIC) simulations [5,6,12,31,76–79].

Negligible current loss was achieved within the Z–accelerator's stack-MITL system between $r = 165$ cm and $r = 80$ cm by taking the following approach: designing the system's four insulator stacks not to flash during the time interval of interest [109]; basing the vacuum-flare designs on the strongly magnetically insulated axisymmetric-vacuum-flare concept described by Refs. [4–7,10,12,16,20,28–35,37–39,82–89]; designing the outer MITLs to be extremely well insulated for most of the electrical power pulse [5,6,10,12,31–33,38,76–79]; minimizing emission of positive ions from the outer-MITL anodes [32,33] by limiting the temperature rise of the anode surfaces to less than 400 K [111]; and minimizing emission of negative ions from the outer-MITL cathodes by not coating the cathode surfaces with graphite or any other substance [112,113].

TABLE II. Measured insulator-stack, MITL, and loss currents for several sets of shots conducted on the Z accelerator. The shots are described in Refs. [37,38]. The measured loss includes that due to insulator flashover at the insulator stacks, MITL-injection current loss between the vacuum flares and outer MITLs, electron-leakage current in the outer MITLs, positive-ion emission from the outer-MITL anodes, and negative-ion emission from the outer-MITL cathodes. For the 90-kV shots, the estimated uncertainty (1σ) in the current loss is 0.4 MA; for the 60-kV shots, the uncertainty is 0.26 MA. Hence for each of the four sets of measurements summarized here, the measured current loss between $r = 165$ cm and $r = 80$ cm is less than the measurement uncertainty.

Z-shot parameters	Z-accelerator Marx-charge voltage	Peak value of the total current at the insulator stack ($r = 165$ cm)	Peak value of the total current in the MITL system ($r = 80$ cm)	Total current loss at peak current, between $r = 165$ cm and $r = 80$ cm
Average of seven nominally identical shots conducted with a 2-cm-length, 2-cm-initial-radius 4.27-mg wire array [38] (Z-shots 51, 52, 540, 541, 619, 685, and 783)	90 kV	20.14 MA	20.34 MA	−0.20 MA
Average of four nominally identical shots conducted with a 1-cm-length, 1-cm-initial-radius 5.88-mg wire array [38] (Z-shots 723, 724, 817, and 818)	90 kV	20.60 MA	20.81 MA	−0.21 MA
Average of two nominally identical shots conducted with a 1-cm-length, 1-cm-initial-radius 2.74-mg wire array [38] (Z-shots 725 and 819)	60 kV	13.06 MA	13.05 MA	0.01 MA
Average of eight nominally identical shots conducted with a 1.2-cm-length 2-cm-initial-radius dynamic hohlraum [37] (Z-shots 1542–1549)	90 kV	21.84 MA	21.65 MA	0.19 MA

We propose to take the same approach to minimize the current loss upstream of the convolute within the Z-300 and Z-800 stack-MITL systems.

As indicated by Table I, the insulator stacks of the Z-300 and Z-800 accelerators are designed to have a flashover probability that is less than 1%. As indicated by Figs. 4 and 12, the vacuum-flare designs of Z 300 and Z 800 are based on the successful concept described by Refs. [4–7,10,12,16,20,28–35,37–39,82–89].

The nominal impedance of the outer-MITL system of the Z accelerator was 0.578 ohms. The nominal impedance of the outer-MITL systems of the Z-300 and Z-800 accelerators is 0.833 ohms. Hence for a given load-inductance time history, the Z-300 and Z-800 outer MITLs will be better magnetically insulated than those of the Z machine.

The temperature of the anode surfaces of an outer-MITL system increases during an accelerator shot due to electron-energy deposition and Ohmic heating. The component of the temperature rise due to electrons can be estimated numerically with circuit [32,33] and particle-in-cell [5,6,12,31,76–79] simulations. Such calculations suggest we limited the temperature rise of Z's outer-MITL anodes to 120 K. For the outer-MITL anodes of Z 300 and Z 800, the temperature rise due to electron-energy deposition is expected to be ∼120 K, since even though Z 300 and Z 800 generate more current, their outer MITLs provide superior magnetic insulation.

The component of the temperature rise due to Ohmic heating can be estimated analytically [114,115]:

$$\Delta\theta = 1.273 \frac{B^2}{2\mu_0 c_v} = 1.273 \frac{\mu_0 j^2}{2c_v}. \qquad (A1)$$

In this expression B is the magnetic field at the conductor surface, $c_v = 3.37 \times 10^6$ [J/(m³K)] is the specific heat of stainless steel (which we use to fabricate MITL electrodes), and j is the lineal current density (in A/m) at the conductor surface. The constant 1.273 assumes the current rises linearly with time; other constants are obtained for different current-pulse time histories [114,115].

According to Eq. (A1), we limited the temperature rise due to Ohmic heating of Z's outer-MITL anode surfaces to 20 K. For the outer-MITL anodes of Z 300 and Z 800, the increases in temperature due to Ohmic heating are estimated to be 20 and 40 K, respectively. Hence the total increases in temperature (due to electron-energy deposition and Ohmic heating) of the outer-MITL anodes of Z 300 and Z 800 are expected to be less than the 400 K required for significant ion emission [111].

The negative-ion current emitted from an uncoated cathode of a conical outer MITL can be estimated as follows. According to Refs. [112,113], the areal current density J_n of negative-ion emission from the cathode of a MITL is proportional to the third power of the lineal density of the current flowing on the cathode surface j:

$$J_n = kj^3 = k\left(\frac{B}{\mu_0}\right)^3 < J_{CL}. \qquad (A2)$$

In this expression k is a constant, B is the magnetic field at the cathode surface, and J_{CL} is the space-charge-limited negative-ion current density. (It is understood that J_n is bounded above by J_{CL}.) Integrating the above equation leads directly to the following expression for the total negative-ion current emitted from a conical MITL cathode:

$$I_n = k\frac{I_k^3}{4\pi^2\cos\vartheta}\left(\frac{1}{r_{min}} - \frac{1}{r_{max}}\right) < I_{CL}. \qquad (A3)$$

The quantity I_n is the total negative ion current, I_k is the MITL-cathode current, ϑ is the angle of the MITL cone with respect to the horizontal, r_{min} is the minimum radius of the cone, r_{max} is the maximum radius, and I_{CL} is the space-charge-limited negative-ion current.

The information provided by Ref. [112] suggests that, for the experimental configuration discussed in [112], the negative-ion current density emitted from an uncoated aluminum MITL cathode is less than 1375 A/m². (Orders of magnitude higher current densities are obtained with a graphite coating [112].) This upper bound was observed at a lineal current density of 1 MA/m. Reference [112] also notes that the geometry used to make the negative-ion-current measurement enhanced the current density by at least a factor of 3 over that which would have been obtained from a system with planar geometry. Hence we conclude from these observations that for an uncoated planar aluminum MITL cathode

$$k < 4.6 \times 10^{-16} (\text{SI units}). \qquad (A4)$$

For the reasons discussed in Ref. [38], we propose to use stainless-steel-304L cathodes for the Z-300 and Z-800 MITLs. The results of [112,113] suggest the cathodes should be uncoated, as were the cathodes described in [38]. Although Eqs. (A2)–(A4) were developed using data acquired with an uncoated aluminum cathode, we tentatively assume these expressions also apply to uncoated stainless steel.

According to Eqs. (A3) and (A4), the peak negative-ion current within the outer-MITL system of the 22-MA Z accelerator was less than 80 kA. The peak negative-ion currents within the outer-MITL systems of Z 300 and Z 800 are expected to be less than 340 and 1000 kA, respectively. Hence current loss due to negative-ion emission within the outer MITLs of Z 300 and Z 800 is expected to be negligible.

APPENDIX B: CURRENT LOSS WITHIN THE CONVOLUTE AND INNER MITL

In this Appendix, we outline a physics model of current loss *within* the post-hole vacuum convolute and inner

MITL of an accelerator such as Z 300 and Z 800, and discuss how this loss can be minimized.

We begin by observing that the outer MITLs, convolute, inner MITL, and load are a coupled system, and that the convolute is a complex three-dimensional device. The MITL-convolute-load systems of the Z-300 and Z-800 accelerators will operate at peak voltages on the order of 10^7 V and peak powers of 10^{14}–10^{15} W. A complete understanding of such a coupled and complex high-voltage, high-power system requires fully relativistic, fully electromagnetic PIC simulations of the time evolution of the system. Such simulations have been conducted and are described in Refs. [5,6,12,31,76–79].

The simulations make clear that current loss within the convolute and inner MITL is carried by charged particles that cross the system's AK gaps. Electrons are emitted from the cathode surfaces of the *outer* MITLs wherever the electric field has exceeded 240 kV/cm [116]. These electrons $\mathbf{E} \times \mathbf{B}$ drift toward the load, and are subsequently lost to the anode surfaces of the convolute and inner MITL [5,6,12,31,76–79]. Although this component of the current loss occurs within the convolute and inner MITL, the current that is lost originates as electron-flow current in the outer MITLs.

Cathode plasma formed by the electron-emission process in the outer MITLs is heated by this process and, in addition, Ohmic heating due to cathode conduction current. As a result, the cathode plasma expands toward the anode surfaces of the outer MITLs [12,77–79,102,103]. Because of this expansion, the effective AK gaps of the outer MITLs decrease with time, which increases the electron-flow current that is launched in the outer MITLs.

As the outer-MITL electron-flow current is lost to the anode surfaces of the convolute and inner MITL, the temperature of these surfaces increases. The anode-surface temperature also increases due to Ohmic heating by anode conduction current. The increased temperature increases the rate of contaminant desorption from these surfaces. The desorbed contaminants expand toward the cathodes of the convolute and inner MITL, become ionized, and serve as a source of positive ions that conduct additional current loss.

Cathode plasma formed by the electron-emission process in the convolute and inner MITL is heated by this process and, in addition, Ohmic heating due to cathode conduction current. As a result, the cathode plasma expands toward the anode surfaces of the convolute and inner MITL [77–79]. The expansion of both the anode and cathode plasmas reduces the system's effective AK gaps, which increases the ion-current loss within the convolute and inner MITL [77–79]. In addition, flow electrons from the outer MITLs fill a significant fraction of the vacuum gaps of the convolute and inner MITL with negative space charge, which enhances the positive-ion current [117].

Particle-in-cell simulations conducted to date [5,6,12,31,76–79] suggest the above physical model of

current loss within the convolute and inner MITL. The simulations also make clear that such a system can be efficient under three conditions: when the characteristic impedance of the load is much less than that of the outer-MITL system; the surfaces of the outer MITLs, convolute, and inner-MITL electrodes are sufficiently clean; and the system's AK gaps are large enough not to close significantly due to the expansion of the system's anode and cathode plasmas during the time interval of interest.

These three conditions are coupled. As the load impedance is reduced, the voltage is reduced and the current is increased throughout the MITL-convolute-load system. This improves magnetic insulation of electrons and ions throughout the system. The increased insulation reduces the amount of electron-flow current that is launched in the outer MITLs and deposited at the anode electrodes of the convolute and inner MITL. The increased insulation also reduces the ion current that is lost within the convolute and inner MITL. As a consequence, the increased insulation increases the amount of surface contamination that can be tolerated, and decreases the minimum allowed AK gaps.

Hence the path to minimizing current loss within the convolute and inner MITL is clear: we must minimize the ratio of load impedance to that of the outer-MITL system; minimize contamination of the electrode surfaces of the outer MITLs, convolute, and inner MITL; and design these components to include sufficiently large AK gaps.

Experiments conducted on the Z accelerator with a dynamic-hohlraum load operated at a peak current of 22 MA achieved negligible current loss in the accelerator's stack-MITL-convolute system [37]. The loss that was measured includes the following components: current loss at the insulator stacks; MITL-injection loss between the vacuum flares and outer MITLs; electron-leakage loss in the outer MITLs; positive-ion and negative-ion emission in the outer MITLs; electron current loss in the double-post-hole vacuum convolute; and positive- and negative-ion current loss in the convolute. The total current loss was so small it was difficult to measure: the observed fractional loss was 0.1% ± 5% [37]. Insulator-stack and inner-MITL current time histories measured on a typical Z shot conducted with a dynamic hohlraum are plotted in Ref. [37] and by Fig. 13(a).

Experiments presently conducted on ZR with a dynamic hohlraum at 26 MA also achieve a negligible total current loss. The measured loss is 3% ± 5%. Insulator-stack and inner-MITL current time histories measured on a typical ZR shot conducted with a dynamic hohlraum are plotted by Fig. 13(b). Both the Z and ZR measurements are consistent with transmission-line-circuit [32,33,38] and fully relativistic, fully electromagnetic PIC simulations [5,6,12,31,76–79].

We have designed the Z-300 and Z-800 accelerators to achieve, with the MagLIF and dynamic-hohlraum loads
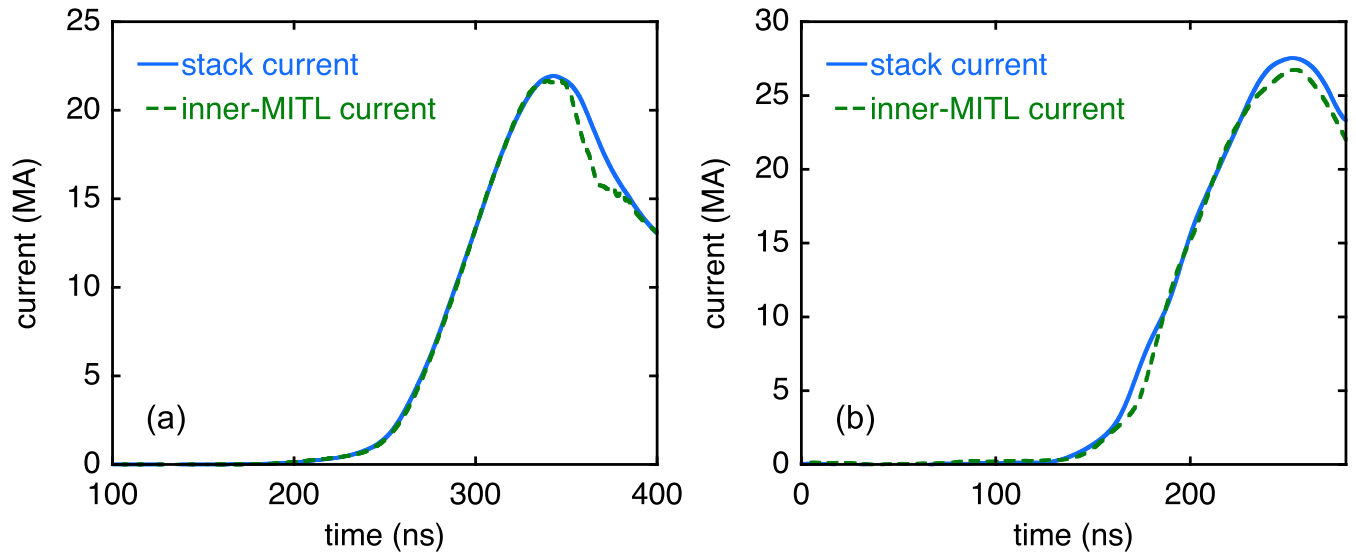
FIG. 13. (a) Measured insulator-stack and inner-MITL currents for Z-shot 1548 [37]. The load on this shot was a dynamic hohlraum. The inner-MITL current was measured 6 cm from the symmetry axis of the load. (b) Measured insulator-stack and inner-MITL currents for ZR-shot 2759, which also drove a dynamic hohlraum. The inner-MITL current was measured at the same distance from the symmetry axis.

described in this article, fractional current losses that are comparable to those achieved by Z and ZR with a dynamic hohlraum. We can estimate analytically the current losses as follows.

As discussed by Sec. III, SCREAMER calculates the MITL-system current loss in a self-consistent manner using Eqs. (31)–(36). Figure 7, which illustrates the model used by SCREAMER, represents the six-level outer-MITL system as an inductor. To estimate the current loss analytically, it is more convenient to use the circuit model given by Fig. 14, which represents the outer-MITL system as a transmission line.

Figure 14 suggests that *at peak load current*, the voltage at the output of the MITL system V_{MITLs} can be expressed as follows (since $dI_k/dt = 0$):
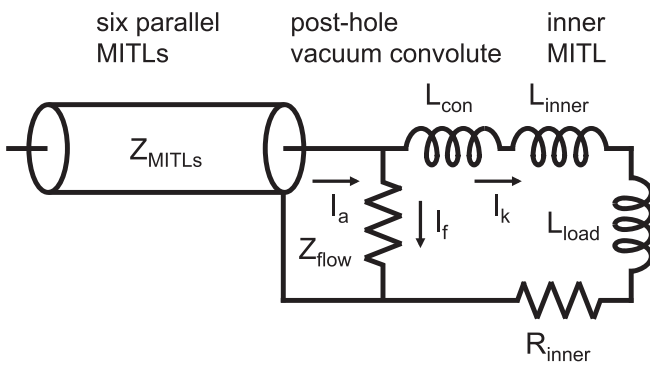

FIG. 14. Idealized circuit model of a coupled MITL-convolute-load system. This model is consistent with that given by Fig. 7, except here we represent the outer-MITL system as a transmission line instead of a lumped inductor.

$$V_{\mathrm{MITLs}} = I_k(Z_{\mathrm{load}} + R_{\mathrm{inner}}), \tag{B1}$$

where

$$Z_{\mathrm{load}} \equiv \frac{dL_{\mathrm{load}}}{dt}\left(\frac{dI_k}{dt} = 0\right). \tag{B2}$$

When $I_{\mathrm{loss}} \ll I_a$, we can combine Eqs. (31)–(36) and (B1) to obtain an estimate for the fractional current loss at peak load current:

$$\frac{I_{\mathrm{loss}}}{I_a} = 1.4\left(\frac{Z_{\mathrm{load}} + R_{\mathrm{inner}}}{Z_{\mathrm{MITLs}}}\right)^2. \tag{B3}$$

[Of course, all the quantities in Eq. (B3) are to be evaluated at peak load current.] This equation assumes all the electron-flow current launched in the outer MITLs is lost to the anode in the vicinity of the convolute. Equation (B3) also assumes that the water flares, insulator stacks, vacuum flares, outer MITLs, convolute, inner MITL, and load are designed and operated in such a manner that this component of the current loss is the dominant loss mechanism. Equation (B3) makes clear that to minimize this current loss requires that we minimize the ratio $(Z_{\mathrm{load}} + R_{\mathrm{inner}})/Z_{\mathrm{MITLs}}$.

For the Z-300 accelerator, we use SCREAMER to estimate $Z_{\mathrm{load}} + R_{\mathrm{inner}}$ at peak load current for the MagLIF and dynamic-hohlraum loads described in this article:

$$\frac{(Z_{\mathrm{load}} + R_{\mathrm{inner}})_{\mathrm{MagLIF}}}{Z_{\mathrm{MITLs}}} = 0.07, \tag{B4}$$

$$\frac{(Z_{\text{load}} + R_{\text{inner}})_{\text{DH}}}{Z_{\text{MITLs}}} = 0.11. \tag{B5}$$

For Z 800,

$$\frac{(Z_{\text{load}} + R_{\text{inner}})_{\text{MagLIF}}}{Z_{\text{MITLs}}} = 0.12, \tag{B6}$$

$$\frac{(Z_{\text{load}} + R_{\text{inner}})_{\text{DH}}}{Z_{\text{MITLs}}} = 0.11. \tag{B7}$$

For the Z accelerator,

$$\frac{(Z_{\text{load}} + R_{\text{inner}})_{\text{DH}}}{Z_{\text{MITLs}}} = 0.16. \tag{B8}$$

For ZR,

$$\frac{(Z_{\text{load}} + R_{\text{inner}})_{\text{DH}}}{Z_{\text{MITLs}}} = 0.13. \tag{B9}$$

The nominal values of Z_{MITLs} for the outer-MITL systems of the Z, ZR, Z-300, and Z-800 machines are 0.578, 0.695, 0.833, and 0.833 Ω, respectively. We note that, for each of the cases considered above, $Z_{\text{load}} \gg R_{\text{inner}}$.

Equations (B1)–(B9) suggest that, at peak load current, the fractional current loss on Z-300 and Z-800 shots (when driving the MagLIF and dynamic-hohlraum loads described in this article) will be comparable to that lost on dynamic-hohlraum shots conducted on Z and ZR. We could reduce the loss further by increasing the value of Z_{MITLs} for Z 300 and Z 800. However, this would increase the MITL-system inductance for each of these two machines. As suggested by Eqs. (C16) and (C22), the increased inductance would increase the stored electrical energy required to deliver a given current to the load, which would increase the size and cost of these accelerators.

Equation (B1) estimates the voltage at the output of the outer-MITL system at peak load current (i.e., when $dI_k/dt = 0$), and hence is independent of L_{con} and L_{inner}. This voltage is used to estimate the fractional current loss at peak load current. It is also of interest to estimate the current loss earlier in time, when dI_k/dt has reached its peak positive value. At this time, the voltage at the output of the outer-MITL system is given approximately by the following expression:

$$V_{\text{MITLs}} = (L_{\text{con}} + L_{\text{inner}})\frac{dI_k}{dt}. \tag{B10}$$

Equation (B10) makes the simplifying assumption that at peak dI_k/dt, the contributions to V_{MITLs} due to the quantities $I_k(dL_{\text{load}}/dt)$, $L_{\text{load}}(dI_k/dt)$, and $I_k R_{\text{inner}}$ can be neglected.

When $I_{\text{loss}} \ll I_a$, we can combine Eqs. (31)–(36) and (B10) to obtain an estimate for the fractional current loss when dI_k/dt has reached its peak positive value:

$$\frac{I_{\text{loss}}}{I_a} = 1.4\left(\frac{(L_{\text{con}} + L_{\text{inner}})(dI_k/dt)}{I_k Z_{\text{MITLs}}}\right)^2. \tag{B11}$$

[Of course, all the quantities in Eq. (B11) are to be evaluated at peak dI_k/dt.] According to Eq. (B11), the fractional current loss on Z 300 and Z 800 will be comparable to that lost on Z and ZR.

We caution that Eqs. (B3) and (B11) are valid only under the idealized assumptions given in Sec. III and this Appendix. For example, it is clear that if the current loss at peak dI_k/dt [as estimated by Eq. (B11)] were sufficiently large, it would cause the AK gaps of the convolute and inner MITL to close significantly before peak current, which would increase the fractional current loss at peak current above that predicted by Eq. (B3). In addition, Eqs. (B3) and (B11) are invalid when the electrode surfaces of the insulator stacks, vacuum flares, outer MITLs, convolute, or inner MITL are sufficiently contaminated; or when the AK gaps of one or more of these components are sufficiently small.

APPENDIX C: ANALYTIC ACCELERATOR-SCALING RELATIONS

An accurate and detailed understanding of the performance of an accelerator (such as Z 300 or Z 800) that generates on the order of a petawatt of peak electrical power in a 100-ns pulse requires accurate and detailed numerical simulations. Developing and optimizing the design of such a machine requires a series of iterative simulations to determine optimum values of accelerator-circuit parameters. Nevertheless, approximate analytic scaling relations can provide useful insight into the operation of such an ultrahigh peak-electrical-power machine. Such relations can also provide *initial* estimates of optimum values of parameters, which can be useful as starting points for the iterative calculations.

To facilitate the development of such analytic relations, we develop in this section an idealized accelerator circuit model, one simpler than that given by Fig. 7. We begin by assuming

$$R_s \ll \sqrt{\frac{L_s}{C_s}}, \tag{C1}$$

$$R_{\text{shunt}} \gg \sqrt{\frac{L_s}{C_s}}, \tag{C2}$$

$$Z_{\text{flow}} \gg Z_{\text{load}}. \tag{C3}$$

We also assume that, from the perspective of the accelerator's impedance-transformer system, the dominant electrical parameter of the accelerator's centrally located vacuum system is its total inductance L_{center}.

The center-section inductance L_{center} is a function of time. We neglect here the time dependence and use instead a characteristic value of the inductance:

$$L_{\text{center}} = L_{\text{stack}} + L_{\text{MITLs}} + L_{\text{con}} + L_{\text{inner}} + L_{\text{load},f}. \quad (C4)$$

The quantities L_{stack}, L_{MITLs}, L_{con}, and L_{inner} are defined in Sec. III. The quantity $L_{\text{load},f}$ is the final load inductance; i.e., the inductance of the load after it has imploded to an arbitrarily specified final radius a_f. For both Z 300 and Z 800, $L_{\text{load},f}$ for a MagLIF liner at a 10:1 convergence ratio is estimated neglecting implosion instabilities:

$$L_{\text{load},f} = 4.61 \text{ nH}. \quad (C5)$$

For both Z 300 and Z 800, $L_{\text{load},f}$ for a dynamic hohlraum is calculated at the time this load has imploded from a radius of 2.0 to 0.3 cm. Coincidentally, this inductance is approximately the same as that of a MagLIF load:

$$L_{\text{load},f} = 4.55 \text{ nH}. \quad (C6)$$

Equation (C4) neglects the increase in the inner-MITL's inductance due to magnetic diffusion and motion of the MITL's vacuum-electrode boundary [104]. (As discussed in Sec. III, both of these effects are accounted for in the circuit model of Fig. 7 by the element R_{inner} [104].)

We make the additional assumption that ρ_w is so high that resistive losses in the water dielectric of the impedance transformers can be neglected. Under this condition and the others given above, Fig. 7 reduces to the idealized circuit given by Fig. 15.

Equations (1), (10), (23), (25), (C1), and (C2) can be used to estimate, for the idealized circuit of Fig. 15, the impedance Z_{in} that maximizes the peak forward-going power delivered by the LTDs to the input of the impedance transformers:

$$Z_s = Z_{\text{in}} = 1.1\sqrt{\frac{L_s}{C_s}} = 1.1 \frac{n_c^2}{n_t}\sqrt{\frac{L_b}{C_b}}. \quad (C7)$$

The power-transport efficiency of the transformer system η_t can be estimated using the results of Ref. [95]:

$$\eta_t \approx \left(1 - \frac{[\ln(Z_{\text{out}}/Z_{\text{in}})]^2}{8\omega\tau_t}\right)^2 \approx \exp\left(\frac{-[\ln(Z_{\text{out}}/Z_{\text{in}})]^2}{4\omega\tau_t}\right), \quad (C8)$$

where ω is the dominant angular frequency of the voltage pulse. The first equation above follows directly from the results presented in [95]. The second equation, given by Ref. [40], simply uses the exponential function to approximate the first equation. Equation (C8) assumes that the impedance of the circuit that drives the transformer system is Z_{in}, the impedance of the load at the output of the system is Z_{out}, and

$$\frac{[\ln(Z_{\text{out}}/Z_{\text{in}})]^2}{4\omega\tau_t} \ll 1. \quad (C9)$$

For the discussion in this Appendix, we make the additional simplifying assumption that the transformer is 100% efficient:

$$\eta_t = 1. \quad (C10)$$

We also assume the LTD modules are transit time isolated from the accelerator's centrally located vacuum section:

$$2\tau_t > \frac{\pi}{\omega}. \quad (C11)$$

Under the conditions given by Eqs. (C1)–(C3), (C7), (C10), and (C11), dimensional analysis makes clear that for the idealized circuit illustrated by Fig. 15, the value of Z_{out} that maximizes the peak electrical power delivered by the transformer system to L_{center} can be a function only of $L_{\text{center}}/(L_s C_s)^{1/2}$, or equivalently $L_{\text{center}}/(L_b C_b)^{1/2}$.
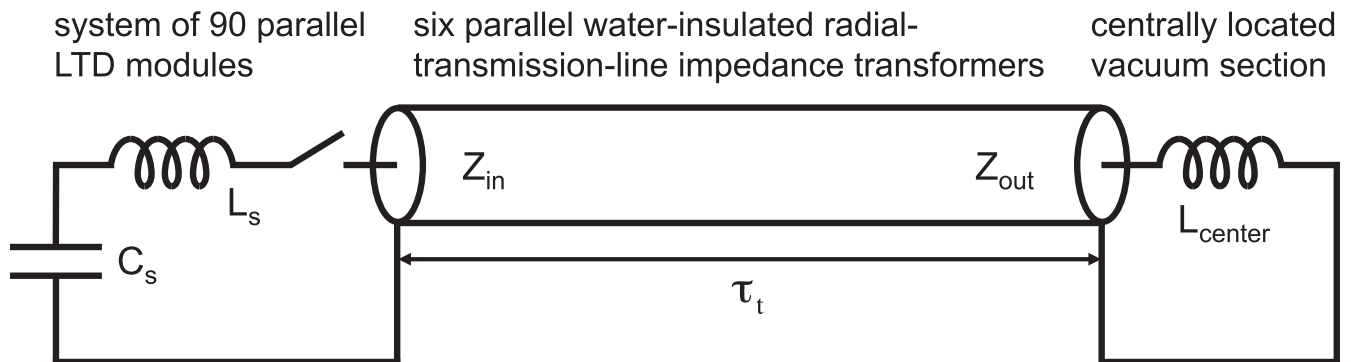

FIG. 15.   Idealized version of the accelerator-circuit model illustrated by Fig. 7.

We use iterative SCREAMER [92,93] simulations to determine numerically this optimum value of Z_{out}:

$$Z_{\text{out}} = 0.88 \frac{L_{\text{center}}}{\sqrt{L_s C_s}} = 0.88 \frac{L_{\text{center}}}{\sqrt{L_b C_b}}. \tag{C12}$$

Equation (C12), which is consistent with Eq. (6) of Ref. [40], can be used to provide an initial estimate for the optimum value of Z_{out} for an accelerator modeled by Fig. 7.

Under the conditions given by Eqs. (C1)–(C3), (C7), and (C10)–(C12), the peak power delivered by the LTD-circuit of Fig. 15 to Z_{in}—and the peak power delivered in turn by the impedance transformers to L_{center}—are the same to within 1%. Dimensional analysis makes clear that both peak powers can be expressed in terms of LTD-system parameters:

$$P_p = 0.30 V_s^2 \sqrt{\frac{C_s}{L_s}} = 0.30 n_t V_b^2 \sqrt{\frac{C_b}{L_b}}. \tag{C13}$$

The constant 0.30 of Eq. (C13) is determined using iterative SCREAMER simulations. The time history of the power delivered to L_{center} is plotted by Fig. 16.

Under the conditions given by Eqs. (C1)–(C3), (C7), and (C10)–(C12), the peak energy delivered to L_{center} is given by the following:

$$E_p = 0.34 C_s V_s^2 = 0.34 n_t C_b V_b^2. \tag{C14}$$

Hence when Z_{out} is chosen to maximize the peak power delivered to L_{center}, only 68% of the energy initially stored by the accelerator's LTD modules [as given by Eq. (8)] can be delivered (in the initial power pulse) by the idealized circuit of Fig. 15 to an inductive load. Under the conditions given by Eqs. (C1)–(C3), (C7), and (C10)–(C12), the peak
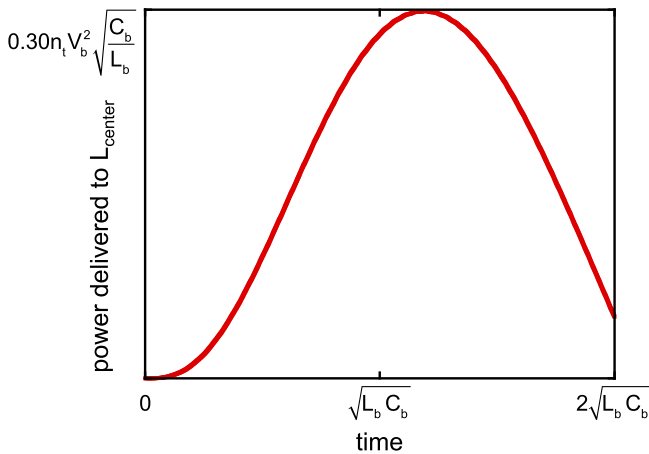
voltage and current, V_p and I_p, respectively, at L_{center} are also readily calculated:

$$V_p = 0.63 V_s \sqrt{\frac{L_{\text{center}}}{L_s}} = 0.63 V_b \sqrt{\frac{n_t L_{\text{center}}}{L_b}}, \tag{C15}$$

$$I_p = 0.82 V_s \sqrt{\frac{C_s}{L_{\text{center}}}} = 0.82 V_b \sqrt{\frac{n_t C_b}{L_{\text{center}}}}. \tag{C16}$$

The time history of the current delivered to L_{center} is plotted by Fig. 17. The 10%–90% rise time of the current pulse delivered to L_{center} is a function of LTD-system parameters:

$$\tau_r = 1.24 \sqrt{L_s C_s} = 1.24 \sqrt{L_b C_b}. \tag{C17}$$

Equations (C12)–(C17) are accurate to within 2% for the idealized circuit illustrated by Fig. 15. These equations are summarized by Table III.

Experimental requirements dictate the requisite value of the current rise time τ_r. Pulsed-power technology places a practical limit on the minimum inductance L_b that can be achieved by an LTD brick. Under these conditions, Eq. (C17) provides an initial estimate for C_b, the requisite capacitance per brick. Experimental requirements also dictate the requisite value of the peak load current I_p. Pulsed-power technology places practical limits on the minimum value of L_{center} and maximum value of V_b. Under these conditions, Eq. (C16) provides an initial estimate of the requisite number of LTD bricks, n_t. Once L_b, C_b, V_b, and n_t are known, Eqs. (8) and (C13) can be used to estimate how much energy needs to be stored by the accelerator's capacitors, and how much electrical power must be generated by the accelerator, to meet the requirements of the experiment.

FIG. 16. Time history of the electrical power delivered to the inductance L_{center} of the idealized accelerator-circuit model illustrated by Fig. 15, assuming Eqs. (C7) and (C12).
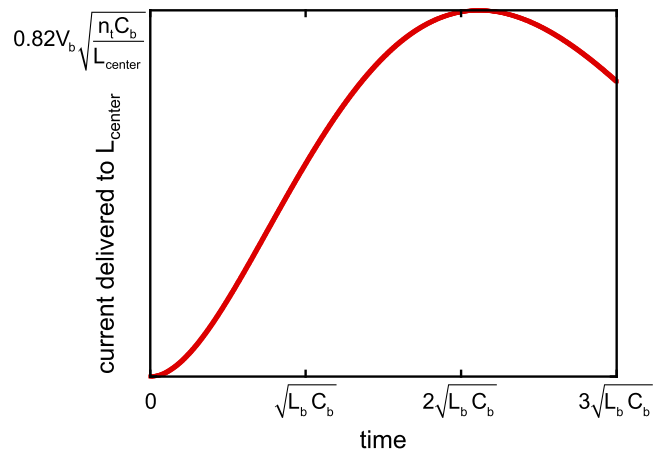

FIG. 17. Time history of the current delivered to the inductance L_{center} of the idealized accelerator-circuit model illustrated by Fig. 15, assuming Eqs. (C7) and (C12).

TABLE III. The peak electrical power P_p, total electrical energy E_p, peak voltage V_p, and peak current I_p at the circuit-element L_{center} of the idealized circuit illustrated by Fig. 15, for two values of Z_{out}. Also given here are the 10%–90% rise times of the current τ_r. When $Z_{\mathrm{out}} = 0.88 L_{\mathrm{center}}/(L_b C_b)^{1/2}$, the peak electrical power delivered to L_{center} is maximized. When $Z_{\mathrm{out}} = 0.55 L_{\mathrm{center}}/(L_b C_b)^{1/2}$, the peak current and electrical energy are maximized. This table demonstrates that the performance of a system consisting of an idealized accelerator coupled to an inductive load is an insensitive function of the accelerator's output impedance Z_{out}. However, as discussed in Appendix C, the lower value of Z_{out} requires a substantially higher electric field at the output of the water-section impedance transformer.

	$Z_{\mathrm{out}} = 0.88 L_{\mathrm{center}}/\sqrt{L_b C_b}$	$Z_{\mathrm{out}} = 0.55 L_{\mathrm{center}}/\sqrt{L_b C_b}$
P_p	$0.30 n_t V_b^2 \sqrt{C_b/L_b}$	$0.28 n_t V_b^2 \sqrt{C_b/L_b}$
E_p	$0.34 n_t C_b V_b^2$	$0.36 n_t C_b V_b^2$
V_p	$0.63 V_b \sqrt{n_t L_{\mathrm{center}}/L_b}$	$0.58 V_b \sqrt{n_t L_{\mathrm{center}}/L_b}$
I_p	$0.82 V_b \sqrt{n_t C_b/L_{\mathrm{center}}}$	$0.85 V_b \sqrt{n_t C_b/L_{\mathrm{center}}}$
τ_r	$1.24\sqrt{L_b C_b}$	$1.39\sqrt{L_b C_b}$

Equation (C12) gives the value of Z_{out} that maximizes the peak electrical *power* delivered by the circuit of Fig. 15 to an inductive load. When Eqs. (C1)–(C3), (C7), (C10), and (C11) are applicable, the value of Z_{out} that maximizes the peak *current* (which also maximizes the peak *energy*) is given by

$$Z_{\mathrm{out}} = 0.55 \frac{L_{\mathrm{center}}}{\sqrt{L_s C_s}} = 0.55 \frac{L_{\mathrm{center}}}{\sqrt{L_b C_b}}. \qquad \text{(C18)}$$

Under the conditions given by Eqs. (C1)–(C3), (C7), (C10), (C11), and (C18), the peak power and energy delivered by the impedance transformers to L_{center} are given by

$$P_p = 0.28 V_s^2 \sqrt{\frac{C_s}{L_s}} = 0.28 n_t V_b^2 \sqrt{\frac{C_b}{L_b}}, \qquad \text{(C19)}$$

$$E_p = 0.36 C_s V_s^2 = 0.36 n_t C_b V_b^2. \qquad \text{(C20)}$$

As expected, the power given by Eq. (C19) is less than that given by Eq. (C13), and the energy given by Eq. (C20) is greater than that given by Eq. (C14).

As indicated by Eqs. (8) and (C20), when Z_{out} is chosen to maximize the current and energy delivered to L_{center}, only 72% of the energy initially stored by the accelerator's LTD modules can be delivered (in the initial power pulse) by the idealized circuit of Fig. 15 to an inductive load.

Under the conditions given by Eqs. (C1)–(C3), (C7), (C10), (C11), and (C18), the peak voltage and current are given by the following expressions:

$$V_p = 0.58 V_s \sqrt{\frac{L_{\mathrm{center}}}{L_s}} = 0.58 V_b \sqrt{\frac{n_t L_{\mathrm{center}}}{L_b}}, \qquad \text{(C21)}$$

$$I_p = 0.85 V_s \sqrt{\frac{C_s}{L_{\mathrm{center}}}} = 0.85 V_b \sqrt{\frac{n_t C_b}{L_{\mathrm{center}}}}. \qquad \text{(C22)}$$

The 10%–90% rise time of the current pulse delivered to L_{center} is given by

$$\tau_r = 1.39\sqrt{L_s C_s} = 1.39\sqrt{L_b C_b}. \qquad \text{(C23)}$$

Equations (C18)–(C23) are accurate to within 2% for the idealized circuit illustrated by Fig. 15. These equations are summarized by Table III.

Equations (C20), (C21), and (C22) [which are obtained assuming Eq. (C18)] *appear* to suggest better accelerator performance than Eqs. (C14), (C15), and (C16) [which are obtained assuming Eq. (C12)]. However, Eqs. (C17) and (C23) indicate that this improvement comes at the expense of a slower rise time. In addition, Eq. (C18) specifies a substantially lower value of Z_{out} than Eq. (C12). The lower impedance requires smaller AK gaps at the output of the transformer system, and consequently higher electric fields. Using the impedance given by Eq. (C18) lowers the peak voltage at the output of the transformers by 8%, as indicated by Eqs. (C15) and (C21); however, Eq. (C18) also specifies that the AK gaps at the output be reduced by 38%, as indicated by comparing Eqs. (C12) and (C18). Hence using Eq. (C18) instead of (C12) increases by 47% the electric fields at the output of the impedance-transformer system.

For the Z-300 and Z-800 accelerators, the value of Z_{out} that optimizes accelerator performance is on the order of the values given by Eqs. (C12) and (C18). Hence these equations can provide initial estimates for the optimum value of Z_{out}.

APPENDIX D: EFFECTIVE PEAK LOAD CURRENT AND LOAD-IMPLOSION TIME

An accelerator design can be evaluated in part by performing a circuit simulation of a hypothetical accelerator shot conducted with an idealized cylindrically symmetric load that undergoes a cylindrical implosion. For such a simulation, two results of interest are the peak current delivered by the accelerator to the load, and the time required for the load to implode.

To enable a comparison of accelerator designs that produce mathematically dissimilar current-pulse shapes, Appendix C of Ref. [40] defines an *effective* peak load current I_{eff} and an *effective* load implosion time $\tau_{i,\mathrm{eff}}$. These quantities are defined as follows:

$$I_{\mathrm{eff}} = 2357 \left(\frac{K_f}{\ell}\right)^{1/2}, \qquad \text{(D1)}$$

$$\tau_{i,\text{eff}} = 4.465 \frac{a_i}{v_f}. \qquad (D2)$$

These expressions apply to a single wire array or liner that undergoes a cylindrical implosion with a 10∶1 convergence ratio. The quantity K_f is the final kinetic energy of the liner at a 10∶1 convergence ratio, and v_f is the final load velocity; i.e., the velocity at a 10∶1 convergence. The constants on the right-hand sides of Eqs. (D1) and (D2) were chosen to give results consistent with those obtained using a circuit simulation of an experiment conducted on the Z accelerator [40].

Equation (D1) guarantees that two simulations with the same effective peak current have the same final pinch kinetic energy per unit length. Equation (D2) guarantees that two simulations with the same initial radius and effective implosion time have the same final pinch velocity.

In this Appendix, we also define the effective peak current and implosion time of a dynamic-hohlraum load, which consists of two nested wire arrays that implode upon a cylindrical foam target located on axis:

$$I_{\text{eff}} = 2676 \left(\frac{K_f}{\ell} \right)^{1/2}, \qquad (D3)$$

$$\tau_{i,\text{eff}} = 3.252 \frac{a_i}{v_f}. \qquad (D4)$$

These expressions are applicable when both the initial radius and mass of the outer array are twice those of the inner array, the initial radius of the outer array is a factor of 6.7 larger than that of the on-axis foam target, and the convergence ratio of the outer array is 6.7∶1.

A more complete discussion of the effective load-current and implosion-time concepts is given by Appendix C of [40].

APPENDIX E: SAFETY AND ENVIRONMENTAL BENEFITS OF LTDS

Reference [40] outlines two machine designs: one powered by Marx generators; the other, LTDs. The conceptual designs of Z 300 and Z 800 presented in this article are based on the LTD-powered option in part because it will be safer for those who work on and in the vicinity of the accelerator, and less impactful to the environment.

The Marx generators described in [40] assume use of 1.34-μF capacitors. Z 300 and Z 800 both assume 80-nF capacitors. According to Ref. [118], a capacitor discharge of 50 J can be sufficient to cause a fatality. At a 100-kV charge voltage, a 1.34-μF capacitor stores 6.7 kJ of energy; an 80-nF capacitor stores 400 J. Of course, any such capacitor must be discharged and kept short-circuited before it can be accessed by a worker; nevertheless, an 80-nF capacitor stores a factor of 17 less energy.

The Marx-generator-based machine described by [40] also assumes use of gas switches insulated by SF$_6$, which is an asphyxiant and a greenhouse gas. Each such switch is triggered by a pulsed 5-MW frequency-quadrupled (266-nm wavelength) Nd∶YAG laser. In contrast to this, the switches assumed by the LTD-based machine are insulated by dry air and electrically triggered. Hence the LTD machine eliminates health and environmental hazards associated with SF$_6$, and eye-safety issues associated with the operation of a large number of pulsed megawatt ultraviolet lasers.

[1] D. B. Reisman, B. S. Stoltzfus, W. A. Stygar, K. N. Austin, E. M. Waisman, R. J. Hickman, J.-P. Davis, T. A. Haill, M. D. Knudson, C. T. Seagle, J. L. Brown, D. A. Goerz, R. B. Spielman, J. A. Goldlust, and W. R. Cravey, Phys. Rev. ST Accel. Beams **18**, 090401 (2015).

[2] J. Deng, W. Xie, S. Feng, M. Wang, H. Li, S. Song, M. Xia, A. He, Q. Tian, Y. Gu, Y. Guan, B. Wei, W. Zou, X. Huang, L. Wang, Z. Zhang, Y. He, and L. Yang, IEEE Trans. Plasma Sci. **41**, 2580 (2013).

[3] E. V. Grabovski, V. P. Smirnov, V. V. Aleksandrov, I. N. Frolov, A. N. Gribov, A. N. Gritsouk, Ya. N. Laukhin, S. F. Medovshikov, K. N. Mitrofanov, G. M. Oleinik, A. A. Samokhin, G. S. Volkov, V. I. Zaitsev, P. V. Sasorov, V. A. Gasilov, O. G. Olkhovskaya, A. P. Shevelko, and V. I. Engelko, at *The 19th IEEE International Pulsed Power Conference* (IEEE, Piscataway, NJ, 2013).

[4] D. H. McDaniel, M. G. Mazarakis, D. E. Bliss, J. M. Elizondo, H. C. Harjes, H. C. Ives, III, D. L. Kitterman, J. E. Maenchen, T. D. Pointon, S. E. Rosenthal, D. L. Smith, K. W. Struve, W. A. Stygar, E. A. Weinbrecht, D. L. Johnson, and J. P. Corley, in *Proceedings of the 5th International Conference on Dense Z Pinches*, edited by J. Davis, C. Deeney, and N. Pereira, AIP Conf. Proc. No. 651 (American Institute of Physics, Melville, NY, 2002), p. 23.

[5] T. D. Pointon and M. E. Savage, in *Proceedings of the 15th IEEE International Pulsed Power Conference*, edited by J. Manechen and E. Schamiloglu (IEEE, Piscataway, NJ, 2005), p. 151.

[6] T. D. Pointon, W. L. Langston, and M. E. Savage, in *Proceedings of the 16th IEEE International Pulsed Power Conference*, edited by E. Schamiloglu and F. Peterkin (IEEE, Piscataway, NJ, 2007), p. 165.

[7] M. E. Savage *et al.*, in *Proceedings of the 16th IEEE International Pulsed Power Conference*, edited by E. Schamiloglu and F. Peterkin (Ref. [6]), p. 979.

[8] K. R. LeChien, M. E. Savage, V. Anaya, D. E. Bliss, W. T. Clark, J. P. Corley, G. Feltz, J. E. Garrity, D. W. Guthrie, K. C. Hodge, J. E. Maenchen, R. Maier, K. R. Prestwich, K. W. Struve, W. A. Stygar, T. Thompson, J. Van Den Avyle, P. E. Wakeland, Z. R. Wallace, and J. R. Woodworth, Phys. Rev. ST Accel. Beams **11**, 060402 (2008).

[9] M. E. Savage and B. S. Stoltzfus, Phys. Rev. ST Accel. Beams **12**, 080401 (2009).

[10] P. A. Corcoran, B. A. Whitney, V. L. Bailey, I. D. Smith, W. A. Stygar, M. E. Savage, G. A. Rochau, J. E. Bailey,

B. M. Jones, T. J. Nash, M. E. Sceiford, L. G. Schlitt, and J. W. Douglas, in *Proceedings of the 17th IEEE International Pulsed Power Conference* (IEEE, Piscataway, NJ, 2009), p. 150.

[11] B. Stoltzfus, K. LeChien, M. Savage, and W. Stygar, in *Proceedings of the 17th IEEE International Pulsed Power Conference* (Ref. [10]), p. 425.

[12] D. V. Rose, D. R. Welch, R. E. Clark, E. A. Madrid, C. L. Miller, C. L. Mostrom, W. A. Stygar, M. E. Cuneo, C. A. Jennings, B. Jones, D. J. Ampleford, and K. W. Struve, in *Proceedings of the 17th IEEE International Pulsed Power Conference* (Ref. [10]), p. 1153.

[13] J. Lips, J. Garde, A. Owen, R. McKee, and W. Stygar, in *Proceedings of the 17th IEEE International Pulsed Power Conference* (Ref. [10]), p. 1266.

[14] D. V. Rose, D. R. Welch, E. A. Madrid, C. L. Miller, R. E. Clark, W. A. Stygar, M. E. Savage, G. A. Rochau, J. E. Bailey, T. J. Nash, M. E. Sceiford, K. W. Struve, P. A. Corcoran, and B. A. Whitney, Phys. Rev. ST Accel. Beams **13**, 010402 (2010).

[15] K. R. LeChien *et al.*, Phys. Rev. ST Accel. Beams **13**, 030401 (2010).

[16] M. E. Savage, K. R. LeChien, M. R. Lopez, B. S. Stoltzfus, W. A. Stygar, D. S. Artery, J. A. Lott, and P. A. Corcoran, in *Proceedings of the 18th IEEE International Pulsed Power Conference*, edited by R. D. Curry and B. V. Oliver (IEEE, Piscataway, NJ, 2011), p. 983.

[17] T. W. L. Sanford *et al.*, Phys. Rev. Lett. **77**, 5063 (1996).

[18] M. K. Matzen, Phys. Plasmas **4**, 1519 (1997).

[19] C. Deeney *et al.*, Phys. Rev. E **56**, 5945 (1997).

[20] R. B. Spielman *et al.*, Phys. Plasmas **5**, 2105 (1998).

[21] D. L. Peterson, R. L. Bowers, K. D. McLenithan, C. Deeney, G. A. Chandler, R. B. Spielman, M. K. Matzen, and N. F. Roderick, Phys. Plasmas **5**, 3302 (1998).

[22] C. Deeney, M. R. Douglas, R. B. Spielman, T. J. Nash, D. L. Peterson, P. L'Eplattenier, G. A. Chandler, J. F. Seamen, and K. W. Struve, Phys. Rev. Lett. **81**, 4883 (1998).

[23] M. A. Liberman, J. S. De Groot, A. Toor, and R. B. Spielman, *Physics of High-Density z-Pinch Plasmas* (Springer, New York, 1999).

[24] D. D. Ryutov, M. S. Derzon, and M. K. Matzen, Rev. Mod. Phys. **72**, 167 (2000).

[25] M. R. Douglas, C. Deeney, R. B. Spielman, C. A. Coverdale, N. F. Roderick, and D. L. Peterson, Phys. Plasmas **7**, 1935 (2000).

[26] M. E. Cuneo *et al.*, Phys. Rev. E **71**, 046406 (2005).

[27] M. C. Jones, D. J. Ampleford, M. E. Cuneo, R. Hohlfelder, C. A. Jennings, D. W. Johnson, B. Jones, M. R. Lopez, J. MacArthur, J. A. Mills, T. Preston, G. A. Rochau, M. Savage, D. Spencer, D. B. Sinars, and J. L. Porter, Rev. Sci. Instrum. **85**, 083501 (2014).

[28] R. B. Spielman, W. A. Stygar, J. F. Seamen, F. Long, H. Ives, R. Garcia, T. Wagoner, K. W. Struve, M. Mostrom, I. Smith, P. Spence, and P. Corcoran, in *Proceedings of the 11th IEEE International Pulsed Power Conference*, edited by G. Cooperstein and I. Vitkovitsky (IEEE, Piscataway, NJ, 1997), p. 709.

[29] K. W. Struve, T. H. Martin, R. B. Spielman, W. A. Stygar, P. A. Corcoran, and J. W. Douglas, in *Proceedings of the 11th IEEE International Pulsed Power Conference*, edited by G. Cooperstein and I. Vitkovitsky (Ref. [28]), p. 162.

[30] I. D. Smith, P. A. Corcoran, W. A. Stygar, T. H. Martin, R. B. Spielman, and R. W. Shoup, in *Proceedings of the 11th IEEE International Pulsed Power Conference*, edited by G. Cooperstein and I. Vitkovitsky (Ref. [28]), p. 168.

[31] M. A. Mostrom, T. P. Hughes, R. E. Clark, W. A. Stygar, and R. B. Spielman, in *Proceedings of the 11th IEEE International Pulsed Power Conference*, edited by G. Cooperstein and I. Vitkovitsky (Ref. [28]), p. 460.

[32] P. A. Corcoran, J. W. Douglas, I. D. Smith, P. W. Spence, W. A. Stygar, K. W. Struve, T. H. Martin, R. B. Spielman, and H. C. Ives, in *Proceedings of the 11th IEEE International Pulsed Power Conference*, edited by G. Cooperstein and I. Vitkovitsky (Ref. [28]), p. 466.

[33] W. A. Stygar *et al.*, in *Proceedings of the 11th IEEE International Pulsed Power Conference, Baltimore*, edited by G. Cooperstein and I. Vitkovitsky (Ref. [28]), p. 591.

[34] H. C. Ives, D. M. Van De Valde, F. W. Long, J. W. Smith, R. B. Spielman, W. A. Stygar, R. W. Wavrick, and R. W. Shoup, in *Proceedings of the 11th IEEE International Pulsed Power Conference*, edited by G. Cooperstein and I. Vitkovitsky (Ref. [28]), p. 1602.

[35] R. W. Shoup, F. Long, T. H. Martin, R. B. Spielman, W. A. Stygar, M. A. Mostrom, K. W. Struve, H. Ives, P. Corcoran, and I. Smith, in *Proceedings of the 11th IEEE International Pulsed Power Conference*, edited by G. Cooperstein and I. Vitkovitsky (Ref. [28]), p. 1608.

[36] R. J. Garcia, H. C. Ives, K. W. Struve, R. B. Spielman, T. H. Martin, M. L. Horry, R. Wavrik, and T. F. Jaramillo, in *Proceedings of the 11th IEEE International Pulsed Power Conference*, edited by G. Cooperstein and I. Vitkovitsky (Ref. [28]), p. 1614.

[37] T. C. Wagoner *et al.*, Phys. Rev. ST Accel. Beams **11**, 100401 (2008).

[38] W. A. Stygar *et al.*, Phys. Rev. ST Accel. Beams **12**, 120401 (2009).

[39] C. A. Jennings, M. E. Cuneo, E. M. Waisman, D. B. Sinars, D. J. Ampleford, G. R. Bennett, W. A. Stygar, and J. P. Chittenden, Phys. Plasmas **17**, 092703 (2010).

[40] W. A. Stygar, M. E. Cuneo, D. I. Headley, H. C. Ives, R. J. Leeper, M. G. Mazarakis, C. L. Olson, J. L. Porter, T. C. Wagoner, and J. R. Woodworth, Phys. Rev. ST Accel. Beams **10**, 030401 (2007).

[41] W. Stygar *et al.*, *Conceptual Designs of 300-TW and 800-TW Pulsed-Power Accelerators* (IEEE, San Francisco, CA, 2013); http://ieeexplore.ieee.org/xpl/articleDetails.jsp?arnumber=6633456.

[42] B. M. Koval'chuk, V. A. Vizir', A. A. Kim, E. V. Kumpyak, S. V. Loginov, A. N. Bastrikov, V. V. Chervyakov, N. V. Tsoi, P. Monjaux, and D. Kh'yui, *Sov. Izw. Vuzov. Phys.* **40**, 25 (1997) [Russ. Phys. J. **40**, 1142 (1997)].

[43] A. N. Bastrikov, V. A. Vizir, S. N. Volkov, V. G. Durakov, A. M. Efremov, V. B. Zorin, A. A. Kim, B. M. Kovalchuk, E. V. Kumpjak, S. V. Loginov, V. A. Sinebryuhov, N. V. Tsou, V. V. Cervjakov, V. P. Yakovlev, and G. A. Meyats, Laser Part. Beams **21**, 295 (2003).

[44] C. L. Olson, Z-pinch inertial fusion energy, in *Landholt-Boernstein Handbook on Energy Technologies, Volume VIII/3 of Fusion Technologies*, edited by W. Martienssen and K. Heinloth (Springer-Verlag, Berlin, 2005).

[45] J. J. Leckbee, J. E. Maenchen, D. L. Johnson, S. Portillo, D. M. Van De Valde, D. V. Rose, and B. V. Oliver, IEEE Trans. Plasma Sci. **34**, 1888 (2006).

[46] D. V. Rose, D. R. Welch, B. V. Oliver, J. J. Leckbee, J. E. Maenchen, D. L. Johnson, A. A. Kim, B. M. Kovalchuk, and V. A. Sinebryukhov, IEEE Trans. Plasma Sci. **34**, 1879 (2006).

[47] W. A. Stygar, W. E. Fowler, K. R. LeChien, F. W. Long, M. G. Mazarakis, G. R. McKee, J. L. McKenney, J. L. Porter, M. E. Savage, B. S. Stoltzfus, D. M. Van De Valde, and J. R. Woodworth, Phys. Rev. ST Accel. Beams **12**, 030402 (2009).

[48] M. G. Mazarakis, W. E. Fowler, A. A. Kim, V. A. Sinebryukhov, S. T. Rogowski, R. A. Sharpe, D. H. McDaniel, C. L. Olson, J. L. Porter, K. W. Struve, W. A. Stygar, and J. R. Woodworth, Phys. Rev. ST Accel. Beams **12**, 050401 (2009).

[49] A. A. Kim, M. G. Mazarakis, V. A. Sinebryukhov, B. M. Kovalchuk, V. A. Visir, S. N. Volkov, F. Bayol, A. N. Bastrikov, V. G. Durakov, S. V. Frolov, V. M. Alexeenko, D. H. McDaniel, W. E. Fowler, K. LeChien, C. Olson, W. A. Stygar, K. W. Struve, J. Porter, and R. M. Gilgenbach, Phys. Rev. ST Accel. Beams **12**, 050402 (2009).

[50] J. R. Woodworth, J. A. Alexander, F. R. Gruner, W. A. Stygar, M. J. Harden, J. R. Blickem, G. J. Dension, F. E. White, L. M. Lucero, H. D. Anderson, L. F. Bennett, S. F. Glover, D. Van De Valde, and M. G. Mazarakis, Phys. Rev. ST Accel. Beams **12**, 060401 (2009).

[51] K. LeChien *et al.*, in *Proceedings of the 17th IEEE International Pulsed Power Conference* (Ref. [10]), p. 1186.

[52] M. G. Mazarakis *et al.*, IEEE Trans. Plasma Sci. **38**, 704 (2010).

[53] J. R. Woodworth, W. A. Stygar, L. F. Bennett, M. G. Mazarakis, H. D. Anderson, M. J. Harden, J. R. Blickem, F. R. Gruner, and R. White, Phys. Rev. ST Accel. Beams **13**, 080401 (2010).

[54] D. V. Rose, C. L. Miller, D. R. Welch, R. E. Clark, E. A. Madrid, C. B. Mostrom, W. A. Stygar, K. R. LeChien, M. A. Mazarakis, W. L. Langston, J. L. Porter, and J. R. Woodworth, Phys. Rev. ST Accel. Beams **13**, 090401 (2010).

[55] A. A. Kim, M. G. Mazarakis, V. I. Manylov, V. A. Vizir, and W. A. Stygar, Phys. Rev. ST Accel. Beams **13**, 070401 (2010).

[56] J. R. Woodworth, W. E. Fowler, B. S. Stoltzfus, W. A. Stygar, M. E. Sceiford, M. G. Mazarakis, H. D. Anderson, M. J. Harden, J. R. Blickem, R. White, and A. A. Kim, Phys. Rev. ST Accel. Beams **14**, 040401 (2011).

[57] T. C. Genoni, D. V. Rose, R. E. Clark, D. R. Welch, and W. A. Stygar, Phys. Rev. ST Accel. Beams **15**, 010401 (2012).

[58] I. D. Smith, Phys. Rev. ST Accel. Beams **7**, 064801 (2004).

[59] F. Gruner, W. Stygar, B. Stoltzfus, J. Woodworth, M. Abdalla, W. Gruner, M. Skipper, and S. Romero, at *The 19th IEEE International Pulsed Power Conference* (Ref. [3]).

[60] S. A. Slutz, M. C. Herrmann, R. A. Vesey, A. B. Sefkow, D. B. Sinars, D. C. Rovang, K. J. Peterson, and M. E. Cuneo, Phys. Plasmas **17**, 056303 (2010).

[61] S. A. Slutz and R. A. Vesey, Phys. Rev. Lett. **108**, 025003 (2012).

[62] R. D. McBride *et al.*, Phys. Rev. Lett. **109**, 135004 (2012).

[63] R. D. McBride *et al.*, Phys. Plasmas **20**, 056309 (2013).

[64] T. J. Awe *et al.*, Phys. Rev. Lett. **111**, 235005 (2013).

[65] T. J. Awe *et al.*, Phys. Plasmas **21**, 056303 (2014).

[66] A. B. Sefkow, S. A. Slutz, J. M. Koning, M. M. Marinak, K. J. Peterson, D. B. Sinars, and R. A. Vesey, Phys. Plasmas **21**, 072711 (2014).

[67] M. R. Gomez *et al.*, Phys. Rev. Lett. **113**, 155003 (2014).

[68] P. F. Schmit *et al.*, Phys. Rev. Lett. **113**, 155004 (2014).

[69] S. A. Slutz, W. A. Stygar, M. R. Gomez, E. M. Campbell, K. J. Peterson, A. B. Sefkow, D. B. Sinars, R. A. Vesey, and R. Betti (to be published).

[70] T. W. L. Sanford, R. E. Olson, R. L. Bowers, G. A. Chandler, M. S. Derzon, D. E. Hebron, R. J. Leeper, R. C. Mock, T. J. Nash, D. L. Peterson, L. E. Ruggles, W. W. Simpson, K. W. Struve, and R. A. Vesey, Phys. Rev. Lett. **83**, 5511 (1999).

[71] D. L. Peterson, R. L. Bowers, W. Matuska, K. D. McLenithan, G. A. Chandler, C. Deeney, M. S. Derzon, M. Douglas, M. K. Matzen, T. J. Nash, R. B. Spielman, K. W. Struve, W. A. Stygar, and N. F. Roderick, Phys. Plasmas **6**, 2178 (1999).

[72] J. E. Bailey *et al.*, Phys. Plasmas **13**, 056301 (2006).

[73] R. W. Lemke, J. E. Bailey, G. A. Chandler, T. J. Nash, S. A. Slutz, and T. A. Mehlhorn, Phys. Plasmas **12**, 012703 (2005).

[74] G. A. Rochau, J. E. Bailey, R. E. Falcon, G. P. Loisel, T. Nagayama, R. C. Mancini, I. Hall, D. E. Winget, M. H. Montgomery, and D. A. Liedahl, Phys. Plasmas **21**, 056308 (2014).

[75] J. E. Bailey *et al.*, Nature (London) **517**, 56 (2015).

[76] T. D. Pointon, W. A. Stygar, R. B. Spielman, H. C. Ives, and K. W. Struve, Phys. Plasmas **8**, 4534 (2001).

[77] D. V. Rose, D. R. Welch, T. P. Hughes, R. E. Clark, and W. A. Stygar, Phys. Rev. ST Accel. Beams **11**, 060401 (2008).

[78] E. A. Madrid, D. V. Rose, D. R. Welch, R. E. Clark, and C. B. Mostrom, W. A. Stygar, M. E. Cuneo, M. R. Gomez, T. P. Hughes, T. D. Pointon, and D. B. Seidel, Phys. Rev. ST Accel. Beams **16**, 120401 (2013).

[79] D. V. Rose, E. A. Madrid, D. R. Welch, R. E. Clark, C. B. Mostrom, W. A. Stygar, and M. E. Cuneo, Phys. Rev. ST Accel. Beams **18**, 030402 (2015).

[80] D. R. Welch (unpublished).

[81] M. E. Savage (unpublished).

[82] D. H. McDaniel, R. W. Stinnett, and I. D. Smith, *Bull. Am. Phys. Soc.* **25**, 1017 (1980).

[83] P. Sincerny, D. Strachan, G. Frazier, C. Gilman, H. Helava, S. Wong, J. Banister, T. DaSilva, S. K. Lam,

D. LePell, J. Levine, R. Rodenburg, and T. Sheridan, in *Proceedings of the 5th IEEE International Pulsed Power Conference*, edited by M. F. Rose and P. J. Turchi (IEEE, Piscataway, NJ, 1985), p. 151.

[84] R. B. Spielman and S. F. Lopez, *Bull. Am. Phys. Soc.* **32**, 1786 (1987).

[85] P. Corcoran, J. Fockler, and D. Wake, Pulse Science Inc. Report No. PSI-FR-390-01, 1988.

[86] P. Corcoran, J. Fockler, H. Kishi, D. Wake, M. Christensen, and R. Sears, Pulse Sciences Inc. Report No. PSI-FR-390-05, 1988.

[87] P. Corcoran and J. Fockler, Pulse Sciences Inc. Report No. PSI-FR-1390-07, 1988.

[88] R. B. Spielman, R. J. Dukart, D. L. Hanson, B. A. Hammel, W. W. Hsing, M. K. Matzen, and J. L. Porter, D. Z. Pinches, in *Proceedings of the 2nd International Conference on Dense Z Pinches*, edited by N. R. Pereira, J. Davis, and N. Rostoker, AIP Conf. Proc. No. 195 (AIP, Melville, New York, 1989), p. 3.

[89] R. B. Spielman, P. Corcoran, J. Fockler, H. Kishi, and P. W. Spence, in *Proceedings of the 7th IEEE International Pulsed Power Conference*, edited by B. H. Bernstein and J. P. Shannon (IEEE, Piscataway, NJ, 1989), p. 445.

[90] G. E. Vogtlin and J. E. Vernazza, in *Proceedings of the 7th IEEE Pulsed Power Conference*, edited by R. White and B. H. Bernstein (IEEE, Piscataway, NJ, 1989), p. 808.

[91] W. A. Stygar *et al.*, Phys. Rev. ST Accel. Beams **8**, 050401 (2005).

[92] M. L. Kiefer and M. M. Widner, in *Proceedings of the 5th IEEE International Pulsed Power Conference*, edited by M. F. Rose and P. J. Turchi (Ref. [83]), p. 685.

[93] R. B. Spielman, M. L. Kiefer, K. L. Shaw, K. W. Struve, and M. M. Widner, SCREAMER, A pulsed power design tool, User's guide for version 3.3.2 (2014).

[94] R. Burdt and R. D. Curry, in *Proceedings of the 16th IEEE International Pulsed Power Conference* (Ref. [6]), p. 302.

[95] I. A. D. Lewis and F. H. Wells, *Millimicrosecond Pulse Techniques* (Pergamon Press, New York, 1959).

[96] D. R. Welch, T. C. Genoni, D. V. Rose, and N. L. Bruner, and W. A. Stygar, Phys. Rev. ST Accel. Beams **11**, 030401 (2008).

[97] W. A. Stygar, T. C. Wagoner, H. C. Ives, P. A. Corcoran, M. E. Cuneo, J. W. Douglas, T. L. Gilliland, M. G. Mazarakis, J. J. Ramirez, J. F. Seamen, D. B. Seidel, and R. B. Spielman, Phys. Rev. ST Accel. Beams **9**, 090401 (2006).

[98] C. W. Mendel, Jr., M. E. Savage, D. M. Zagar, W. W. Simpson, T. W. Grasser, and J. P. Quintenz, J. Appl. Phys. **71**, 3731 (1992).

[99] C. W. Mendel, Jr. and S. E. Rosenthal, Phys. Plasmas **2**, 1332 (1995).

[100] C. W. Mendel, Jr. and S. E. Rosenthal, Phys. Plasmas **3**, 4207 (1996).

[101] C. W. Mendel, Jr. and D. B. Seidel, Phys. Plasmas **6**, 4791 (1999).

[102] B. T. Hutsel, B. S. Stoltzfus, W. E. Fowler, P. A. Jones, D. W. Justus, K. R. LeChien, F. W. Long, D. J. Lucero, K. A. MacRunnels, M. G. Mazarakis, J. L. McKenney, J. K. Moore, T. D. Mulville, J. L. Porter, M. E. Savage, and W. A. Stygar, Sandia National Laboratories Report No. SAND2014-17769, 2014.

[103] C. Thoma, T. C. Genoni, D. R. Welch, D. V. Rose, R. E. Clark, C. L. Miller, W. A. Stygar, and M. L. Kiefer, Phys. Plasmas **22**, 032101 (2015).

[104] W. A. Stygar, S. E. Rosenthal, H. C. Ives, T. C. Wagoner, G. O. Allshouse, K. E. Androlewicz, G. L. Donovan, D. L. Fehl, M. H. Frese, T. L. Gilliland, M. F. Johnson, J. A. Mills, D. B. Reisman, P. G. Reynolds, C. S. Speas, R. B. Spielman, K. W. Struve, A. Toor, and E. M. Waisman, Phys. Rev. ST Accel. Beams **11**, 120401 (2008).

[105] W. A. Stygar *et al.*, Phys. Rev. E **69**, 046403 (2004).

[106] W. A. Stygar *et al.*, Phys. Rev. E **72**, 026404 (2005).

[107] W. A. Stygar, T. C. Wagoner, H. C. Ives, Z. R. Wallace, V. Anaya, J. P. Corley, M. E. Cuneo, H. C. Harjes, J. A. Lott, G. R. Mowrer, E. A. Puetz, T. A. Thompson, S. E. Tripp, J. P. VanDevender, and J. R. Woodworth, Phys. Rev. ST Accel. Beams **9**, 070401 (2006).

[108] W. A. Stygar, M. E. Savage, T. C. Wagoner, L. F. Bennett, J. P. Corley, G. L. Donovan, D. L. Fehl, H. C. Ives, K. R LeChien, G. T. Leifeste, F. W. Long, R. G. McKee, J. A. Mills, J. K. Moore, J. J. Ramirez, B. S. Stoltzfus, K. W. Struve, and J. R. Woodworth, Phys. Rev. ST Accel. Beams **12**, 010402 (2009).

[109] W. A. Stygar *et al.*, Phys. Rev. ST Accel. Beams **7**, 070401 (2004).

[110] H. N. Woodall and R. W. Stinnett, in *Proceedings of the 5th IEEE International Pulsed Power Conference*, edited by M. F. Rose and P. J. Turchi (Ref. [83]), p. 499.

[111] T. W. L. Sanford, J. A. Halbleib, J. W. Poukey, A. L. Pregenzer, R. C. Pate, C. E. Heath, R. Mock, G. A. Mastin, D. C. Ghiglia, T. J. Roemer, P. W. Spence, and G. A. Proulx, J. Appl. Phys. **66**, 10 (1989).

[112] R. W. Stinnett and T. Stanley, J. Appl. Phys. **53**, 3819 (1982).

[113] R. W. Stinnett and M. T. Buttram, J. Fusion Energy **3**, 253 (1983).

[114] H. Knoepfel, *Pulsed High Magnetic Fields* (North-Holland, London, 1970).

[115] H. E. Knoepfel, *Magnetic Fields* (Wiley, New York, 2000).

[116] M. S. Di Capua and D. G. Pellinen, J. Appl. Phys. **50**, 3713 (1979).

[117] M. P. Desjarlais, Phys. Rev. Lett. **59**, 2295 (1987).

[118] *CRC Handbook of Tables for Applied Engineering Science*, edited by R. E. Bolz and G. L. Tuve (CRC Press, Boca Raton, Florida, 1979), p. 790.